Journal of Mathematical Chemistry, Vol. 42, No. 3, October 2007 (© 2006)
DOI: 10.1007/s10910-006-9128-3

Group-theoretical foundations for the concept of mandalas as diagrammatical expressions for characterizing symmetries of stereoisomers

Shinsaku Fujita

Department of Chemistry and Materials Technology, Kyoto Institute of Technology, Matsugasaki, Sakyoku, Kyoto 606-8585, Japan
E-mail: fujitas@chem.kit.ac.jp

Received 13 march 2006; revised 5 April 2006

Group-theoretical foundations for the concept of mandalas have been formulated algebraically and diagrammatically in order to reinforce the spread of the unit-subduced-cycle-index (USCI) approach (S. Fujita, *Symmetry and Combinatorial Enumeration in Chemistry*, Springer-Verlag, Berlin-Heidelberg, 1991). Thus, after the introducton of right coset representations (RCR) (**H**\)**G** and left coset representations (LCR) **G**(/**H**) for the group **G** and its subgroup **H**, a regular body of **G**-symmetry is defined as a diagrammatical expression for a right regular representation ($\mathbf{C}_1$\)**G**, which is an extreme case of RCRs. The |**G**| substitution positions of the regular body as a reference are numbered in accord with the numbering of the elements of **G** and segmented into |**G**|/|**H**| of **H**-segments, which are governed by the RCR (**H**\)**G**. By regarding each **H**-segment as a substitution position, the **H**-segmented regular body is reduced into a reduced regular body, which can be regarded as a secondary skeleton for generating a molecule. The reference regular body (or **H**-segmented one) is operated by every symmetry operations of **G** to generate regular bodies (or **H**-segmented ones), which are placed on the vertices of a hypothetical regular body of **G**-symmetry. The resulting diagram (a nested regular body) is called *a mandala* (or a reduced mandala), which is a diagrammatical expression for specifying the **G**-symmetry of a molecule. The effect of a **K**-subduction on the regular bodies of a mandala (or a reduced mandala) results in the **K**-assemblage of the mandala (or the reduced mandala), where the resulting **K**-assemblies governed by the LCR **G**(/**K**) construct a |**G**|/|**K**|-membered orbit, which corresponds to a molecule of **K**-symmetry. The sphericity of the RCR (or the LCR) is used to characterize symmetrical properties of substitution positions and those of stereoisomers. The fixed-point vector for each mandala (or reduced mandala) in terms of row view and the number of fixed points of **K**-assembled mandalas (or **K**-assembled reduced mandalas) in terms of column view are compared to accomplish combinatorial enumeration of stereoisomers. The relationship between a mandala and a reordered multiplication table is discussed.

KEY WORDS: mandala, regular body, segmentation, assemblage, sphericity, coset representation

1. Introduction

Stereochemistry in a broader meaning contains two main fields, i.e., intramolecular stereochemistry (i.e., stereochemistry in a narrower meaning) and intermolecular stereochemistry (i.e., stereoisomerism). These fields are so closely related to each other that such terms as "enantiotopic", "diastereotopic", and "stereoheterotopic" for the former field of stereochemistry have been coined after such terms as "enantiomeric", "diastereomeric", and "stereoisomeric" for stereoisomerism [1–3]. However, the close relationship has been discussed only in a descriptive manner in most conventional textbooks on stereochemistry [4–7]. In particular, a common mathematical framework to be applied to both of the fields has not been so fully developed that chemical combinatorics for enumerating stereoisomers have not gained popularity, although there have been reported several pioneering works [8–11].

To pursue such a common mathematical framework, we have developed the unit-subduced-cycle-index (USCI) approach [12], where the concept of *sphericity* has been shown to be a key concept for comprehending intramolecular stereochemistry and stereoisomerism. The concept of sphericity has been applied successfully to descriptive stereochemistry (both intramolecular stereochemistry and stereoisomerism) [13, 14] as well as to chemical combinatorics [15–17]. The versatility of the USCI approach based on the sphericity concept in both of the fields of stereochemistry has been summarized in recent reviews [18–20].

In spite of the potentiality of the USCI approach for organic chemists, barriers to access to it have been pointed out in a book review [21] on Fujita's monograph on the USCI approach [12] and have been recently referred to as "an organic chemistry paradox in the Era of Fujita" in a book [22] and in a review [23]. To remove such barriers, we have reported a more intuitive definition of the sphericity concept in order to aim mainly at systematizing intramolecular stereochemistry [24, 25]. By following the intuitive definition, the importance of the sphericity concept has been discussed for introductory courses of stereochemistry [26, 27].

On the other hand, the USCI approach to stereoisomerism (intermolecular stereochemistry) has been visualized in terms of "graphical models"[23, 28–30]. The visualization due to the graphical models, however, has not fully demonstrated the common mathematical framework covering both of the fields. Moreover, the visualization has not explicitly involved the concept of sphericity so that it has not directly aimed at stereoisomer enumeration, one of the most important disciplines accomplished by Fujita's USCI approach. In order to clarify the usefulness of the sphericity concept in the stereoisomer enumeration as well as to demonstrate the common mathematical framework covering both of the fields, we have proposed the concept of *mandalas*, which are diagrammatical expressions of stereoisomers [31–33]. However, the original disclosure for defining the concept of mandalas is rather intuitive because of the didactic purpose of the

papers [31–33]. It is desirable to provide more group-theoretical foundations in order that we will go on further discussions or applications of the mandala concept.

The present paper will demonstrate group-theoretical foundations for the concept of mandalas as diagrammatical expressions of stereoisomers. In particular, right and left coset representations (LCR) derived from multiplication tables of groups will be discussed to introduce the concept of mandalas. Thereby, the sphericity concept will be demonstrated in a renewed fashion in connection with the mandala concept.

2. Coset representations, marks, and sphericities

Before we will propose group-theoretical foundations for the concept of *mandala*, we shall discuss coset representation and marks, which are rather old mathematical concepts introduced by Burnside [34] but revived recently to discuss stereochemistry [12]. A new matter added in this section is a theoretically meaningful discrimination between right and left coset representations, which have been usually regarded as equivalent in the traditional group theory. In addition, this section is devoted to introduce the concepts of sphericity and sphericity indices, which give a theoretical basis of Fujita's USCI approach [12] for integrating intramolecular stereochemistry, stereoisomerism, and chemical combinatorics.

2.1. Right and left coset representations

Let the symbol **G** represent a group of finite order ($|\mathbf{G}|$). Then, its subgroup **H** of order $|\mathbf{H}|$ causes a partition of the group **G** so as to generate a right coset decomposition:

$$\mathbf{G} = \mathbf{H}g_1 + \mathbf{H}g_2 + \cdots + \mathbf{H}g_r, \tag{1}$$

where we place $g_1 = I$ and $r = |\mathbf{G}|/|\mathbf{H}|$. Thereby, a set of right cosets $\mathbf{H}\backslash\mathbf{G}$ is constructed as follows:

$$\mathbf{H}\backslash\mathbf{G} = \{\mathbf{H}g_1, \mathbf{H}g_2, \ldots, \mathbf{H}g_r\}. \tag{2}$$

When each of the right cosets is multiplied by an operation g ($\in \mathbf{G}$) from the right-side direction, the following permutation is obtained:

$$g \sim \begin{pmatrix} \mathbf{H}g_1 & \mathbf{H}g_2 & \cdots & \mathbf{H}g_r \\ \mathbf{H}g_1 g & \mathbf{H}g_2 g & \cdots & \mathbf{H}g_r g \end{pmatrix}, \tag{3}$$

$$\sim \begin{pmatrix} 1 & 2 & \cdots & r \\ t_{g1}^{[R]} & t_{g2}^{[R]} & \cdots & t_{gr}^{[R]} \end{pmatrix} = p_g^{[R]}, \tag{4}$$

where the degree of each permutation is equal to $r = |\mathbf{G}|/|\mathbf{H}|$. When g runs over $\mathbf{G}$, the permutation $p_g^{[R]}$ constructs a set of permutations:

$$(\mathbf{H}\backslash)\mathbf{G} = \{p_g^{[R]} \mid \forall g \in \mathbf{G}\}, \tag{5}$$

which is called *a right coset representation* (RCR) of $\mathbf{G}$ modulo $\mathbf{H}$. Note that, although the symbol $\mathbf{G}(/\mathbf{H})$ is used to designate right cosets in Fujita's book [12], the present paper adopts the symbol $(\mathbf{H}\backslash)\mathbf{G}$ in order to discriminate right cosets from left cosets.

On the same line, a subgroup $\mathbf{K}$ of order $|\mathbf{K}|$ causes a left coset decomposition,

$$\mathbf{G} = \tilde{g}_1\mathbf{K} + \tilde{g}_2\mathbf{K} + \cdots + \tilde{g}_s\mathbf{K}, \tag{6}$$

where we place $\tilde{g}_1 = I$ and $s = |\mathbf{G}|/|\mathbf{K}|$. Thereby, we construct a set of left cosets $\mathbf{G}/\mathbf{K}$ as follows:

$$\mathbf{G}/\mathbf{K} = \{\tilde{g}_1\mathbf{K}, \tilde{g}_2\mathbf{K}, \ldots, \tilde{g}_s\mathbf{K}\}. \tag{7}$$

When each of the left cosets is multiplied by an operation g ($\in \mathbf{G}$) from the left-side direction, the following permutation is obtained:

$$g \sim \begin{pmatrix} \tilde{g}_1\mathbf{K} & \tilde{g}_2\mathbf{K} & \cdots & \tilde{g}_s\mathbf{K} \\ g\tilde{g}_1\mathbf{K} & g\tilde{g}_2\mathbf{K} & \cdots & g\tilde{g}_s\mathbf{K} \end{pmatrix}, \tag{8}$$

$$\sim \begin{pmatrix} 1 & 2 & \cdots & r \\ t_{\tilde{g}_1}^{[L]} & t_{\tilde{g}_2}^{[L]} & \cdots & t_{\tilde{g}_s}^{[L]} \end{pmatrix} = p_g^{[L]}, \tag{9}$$

where the degree of each permutation is equal to $s = |\mathbf{G}|/|\mathbf{K}|$. When g runs over $\mathbf{G}$, the permutation $p_g^{[L]}$ constructs a set of permutations:

$$\mathbf{G}(/\mathbf{K}) = \{p_g^{[L]} \mid \forall g \in \mathbf{G}\}, \tag{10}$$

which is called *a* (LCR) of $\mathbf{G}$ modulo $\mathbf{K}$.

Example 1. This example on the point group $\mathbf{D}_{2d}$ for an allene skeleton is based on Chapters 2 and 5 of Fujita's book [12].

The eight symmetry operations of $\mathbf{D}_{2d}$ are shown in figure 1. They construct the $\mathbf{D}_{2d}$ point group as follows:

$$\mathbf{D}_{2d} = \{\underbrace{I}_{1}, \underbrace{C_{2(1)}}_{2}, \underbrace{C_{2(2)}}_{3}, \underbrace{C_{2(3)}}_{4}; \underbrace{\sigma_{d(1)}}_{5}, \underbrace{S_4}_{6}, \underbrace{S_4^3}_{7}, \underbrace{\sigma_{d(2)}}_{8}\}, \tag{11}$$

which is closed with respect to the multiplication of the operations, as shown in the corresponding multiplication table (figure 2). For the sake of convenience, the symmetry operations are sequentially numbered in accord with the appearance order of equation (11).

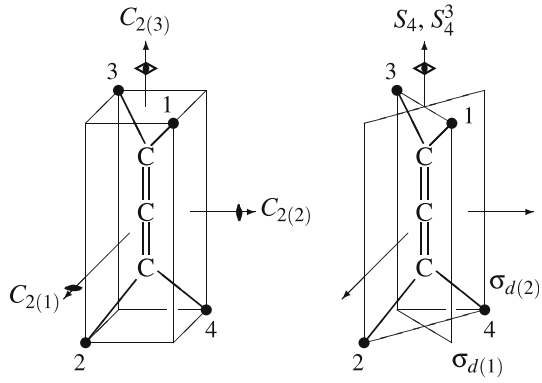

Figure 1. Symmetry operations of an allene molecule. Proper rotations are depicted in the left diagram, while improper rotations (rotoreflections) are depicted in the right diagram. The left diagram shows three twofold rotations ($C_{2(1)}$, $C_{2(2)}$, and $C_{2(3)}$) around symmetry axes, which are perpendicular to one another as designated by vector symbols. The three twofold rotations and an identity operation (I) are referred to as *proper rotations*. The right diagram shows rotoreflections, which are two mirror reflections ($\sigma_{d(1)}$ and $\sigma_{d(2)}$) and two fourfold rotoreflections (S_4 and S_4^3). They are referred to as *improper rotations*.

second operation		first operation: 1	2	3	4	5	7	6	8
		I	$C_{2(1)}$	$C_{2(2)}$	$C_{2(3)}$	$\sigma_{d(1)}$	S_4^3	S_4	$\sigma_{d(2)}$
1	I	1	2	3	4	5	7	6	8
2	$C_{2(1)}$	2	1	4	3	7	5	8	6
3	$C_{2(2)}$	3	4	1	2	6	8	5	7
4	$C_{2(3)}$	4	3	2	1	8	6	7	5
5	$\sigma_{d(1)}$	5	6	7	8	1	3	2	4
6	S_4	6	5	8	7	3	1	4	2
7	S_4^3	7	8	5	6	2	4	1	3
8	$\sigma_{d(2)}$	8	7	6	5	4	2	3	1

Figure 2. Multiplication table of $\mathbf{D}_{2d}$.

Among the subsets of the $\mathbf{D}_{2d}$, there are subsets which are closed by the same multiplication. They are called *subgroups*:

$$\mathbf{D}_2 = \{I, C_{2(3)}, C_{2(1)}, C_{2(2)}\}, \tag{12}$$

$$\mathbf{C}_{2v} = \{I, C_{2(3)}; \sigma_{d(1)}, \sigma_{d(2)}\}, \tag{13}$$

$$\mathbf{S}_4 = \{I, C_{2(3)}; S_4, S_4^3\}, \tag{14}$$

$$\mathbf{C}_2 = \{I, C_{2(3)}\}, \tag{15}$$

$$\mathbf{C}_2' = \{I, C_{2(1)}\}, \qquad \mathbf{C}_2'' = \{I, C_{2(2)}\}, \tag{16}$$

$$\mathbf{C}_s = \{I, \sigma_{d(1)}\}, \qquad \mathbf{C}_s' = \{I, \sigma_{d(2)}\}, \tag{17}$$

$$\mathbf{C}_1 = \{I\}. \tag{18}$$

Among them, $\mathbf{C}_2'$ and $\mathbf{C}_2''$ are conjugate to each other, because the corresponding two-fold axes are superposable by an operator of $\mathbf{D}_{2d}$. This feature is designated by the equation: $S_4^{-1}\mathbf{C}_2'S_4 = \mathbf{C}_2''$. Similarly, $\mathbf{C}_s$ and $\mathbf{C}_s'$ are conjugate to each other because the corresponding mirror planes are superposable by an operator of $\mathbf{D}_{2d}$. This feature is designated by the equation: $S_4^{-1}\mathbf{C}_sS_4 = \mathbf{C}_s'$.

Among these subgroups, a non-redundant set of subgroups ($\mathrm{SSG}_{\mathbf{D}_{2d}}$) is selected as follows:

$$\mathrm{SSG}_{\mathbf{D}_{2d}} = \{\mathbf{C}_1, \mathbf{C}_2, \mathbf{C}_2', \mathbf{C}_s, \mathbf{S}_4, \mathbf{D}_2, \mathbf{D}_{2d}\}, \tag{19}$$

where the alignment is in an ascending order of the orders of the subgroups and an appropriate representative is adopted if conjugate subgroups are present.

Example 2. This example on the RCR $(\mathbf{C}_s\backslash)\mathbf{D}_{2d}$ is essentially based on Chapter 2 of Fujita's book [12], although the present notation is slightly different from the original one. By starting from equation (11), we obtain the corresponding right coset decomposition as follows:

$$\mathbf{D}_{2d} = \mathbf{C}_s + \mathbf{C}_sC_{2(1)} + \mathbf{C}_sC_{2(3)} + \mathbf{C}_sC_{2(2)} \tag{20}$$

$$= \underbrace{\{1, 5\}}_{1} + \underbrace{\{2, 6\}}_{2} + \underbrace{\{4, 8\}}_{3} + \underbrace{\{3, 7\}}_{4}, \tag{21}$$

where the numbering of the symmetry operations contained in each coset is shown in figure 2. Then, the following set of right cosets is obtained:

$$\mathbf{C}_s\backslash\mathbf{D}_{2d} = \{\underbrace{\mathbf{C}_s}_{1}, \underbrace{\mathbf{C}_sC_{2(1)}}_{2}, \underbrace{\mathbf{C}_sC_{2(3)}}_{3}, \underbrace{\mathbf{C}_sC_{2(2)}}_{4}\}, \tag{22}$$

where these cosets are numbered sequentially from 1 to 4. Note that an arbitrary mode of numbering can be selected for equation (22) from the 4! ways of numbering without losing generality. However, it is convenient to select an adequate mode of numbering to satisfy the correspondence to the numbering of positions shown in figure 1. When each coset is multiplied by g ($\in \mathbf{D}_{2d}$), the following permutation is obtained:

$$g \overset{[R]}{\sim} \begin{pmatrix} \mathbf{C}_s & \mathbf{C}_sC_{2(1)} & \mathbf{C}_sC_{2(3)} & \mathbf{C}_sC_{2(2)} \\ \mathbf{C}_sg & \mathbf{C}_sC_{2(1)}g & \mathbf{C}_sC_{2(3)}g & \mathbf{C}_sC_{2(2)}g \end{pmatrix} \tag{23}$$

$$\sim \begin{pmatrix} 1 & 2 & 3 & 4 \\ t_{g1}^{[R]} & t_{g2}^{[R]} & t_{g3}^{[R]} & t_{g4}^{[R]} \end{pmatrix} = p_g^{[R]}. \tag{24}$$

When g runs over $\mathbf{D}_{2d}$, the resulting permutations generate a RCR as follows:

$$(\mathbf{C}_s\backslash)\mathbf{D}_{2d} = \{p_g^{[R]} \mid \forall g \in \mathbf{D}_{2d}\}, \tag{25}$$

which is transitive under $\mathbf{D}_{2d}$. For the sake of convenience, each $p_g^{[R]}$ is expressed as a product of cycles, e.g.,

$$C_{2(1)} \overset{[R]}{\sim} \begin{pmatrix} \mathbf{C}_s I & \mathbf{C}_s C_{2(1)} & \mathbf{C}_s C_{2(3)} & \mathbf{C}_s C_{2(2)} \\ \mathbf{C}_s C_{2(1)} & \mathbf{C}_s I & \mathbf{C}_s C_{2(2)} & \mathbf{C}_s C_{2(3)} \end{pmatrix} \tag{26}$$

$$\sim p_{C_{2(1)}}^{[R]} = \begin{pmatrix} 1\ 2\ 3\ 4 \\ 2\ 1\ 4\ 3 \end{pmatrix} = (1\ 2)(3\ 4), \tag{27}$$

where (1 2) and (3 4) represent cycles to show the transformations of the relevant right cosets. The concrete form of the RCR $(\mathbf{C}_s\backslash)\mathbf{D}_{2d}$ is calculated as follows:

$$I \sim \begin{pmatrix} 1\ 2\ 3\ 4 \\ 1\ 2\ 3\ 4 \end{pmatrix} = (1)(2)(3)(4), \tag{28}$$

$$C_{2(1)} \sim \begin{pmatrix} 1\ 2\ 3\ 4 \\ 2\ 1\ 4\ 3 \end{pmatrix} = (1\ 2)(3\ 4), \tag{29}$$

$$C_{2(2)} \sim \begin{pmatrix} 1\ 2\ 3\ 4 \\ 4\ 3\ 2\ 1 \end{pmatrix} = (1\ 4)(2\ 3), \tag{30}$$

$$C_{2(3)} \sim \begin{pmatrix} 1\ 2\ 3\ 4 \\ 3\ 4\ 1\ 2 \end{pmatrix} = (1\ 3)(2\ 4), \tag{31}$$

$$\sigma_{d(1)} \sim \begin{pmatrix} 1\ 2\ 3\ 4 \\ \bar{1}\ 4\ \bar{3}\ \bar{2} \end{pmatrix} = \overline{(1)(3)(2\ 4)}, \tag{32}$$

$$S_4 \sim \begin{pmatrix} 1\ 2\ 3\ 4 \\ \bar{2}\ \bar{3}\ \bar{4}\ \bar{1} \end{pmatrix} = \overline{(1\ 2\ 3\ 4)}, \tag{33}$$

$$S_4^3 \sim \begin{pmatrix} 1\ 2\ 3\ 4 \\ \bar{4}\ \bar{1}\ \bar{2}\ \bar{3} \end{pmatrix} = \overline{(1\ 4\ 3\ 2)}, \tag{34}$$

$$\sigma_{d(2)} \sim \begin{pmatrix} 1\ 2\ 3\ 4 \\ \bar{3}\ \bar{2}\ \bar{1}\ \bar{4} \end{pmatrix} = \overline{(1\ 3)(2)(4)}, \tag{35}$$

where an overbar represents the invertion of one chirality into an opposite chirality. These permutations of $(\mathbf{C}_s\backslash)\mathbf{D}_{2d}$ control the symmetrical behavior of the four positions of the allene skeleton shown in figure 1. In other words, the RCR $(\mathbf{C}_s\backslash)\mathbf{D}_{2d}$ governs the orbit (equivalence class) of the four positions in the allene skeleton.

Let us consider an operation a satisfying $a \in \mathbf{H}g_i$ ($i = 1, 2, \ldots,$ or r in equation (1)). Then, we obtain $ag_i^{-1} \in \mathbf{H}$. Because $\mathbf{H}$ is a group, the inverse of ag_i^{-1} is also an element of $\mathbf{H}$, i.e., $(ag_i^{-1})^{-1} \in \mathbf{H}$. This means $g_i a^{-1} \in \mathbf{H}$, i.e., $a^{-1} \in g_i^{-1}\mathbf{H}$. By running g_i over the transversal of representatives of equation (1), we obtain the corresponding left coset decomposition:

$$\mathbf{G} = g_1^{-1}\mathbf{H} + g_2^{-1}\mathbf{H} + \cdots + g_r^{-1}\mathbf{H}, \tag{36}$$

where we place $g_1^{-1} = I$ and $r = |\mathbf{G}|/|\mathbf{H}|$. Note that the right coset $\mathbf{H}g_i$ (equation (1)) corresponds to the left coset $g_i^{-1}\mathbf{H}$ (equation (36)) in one-to-one fashion. Thereby, we derive the following set of lefts cosets from equation (36),

$$\mathbf{G}/\mathbf{H} = \{g_1^{-1}\mathbf{H}, g_2^{-1}\mathbf{H}, \ldots, g_r^{-1}\mathbf{H}\}. \tag{37}$$

On the same line as equations (3) and (4), we obtain the following permutation:

$$g \sim \begin{pmatrix} g_1^{-1}\mathbf{H} & g_2^{-1}\mathbf{H} & \cdots & g_r^{-1}\mathbf{H} \\ gg_1^{-1}\mathbf{H} & gg_2^{-1}\mathbf{H} & \cdots & gg_r^{-1}\mathbf{H} \end{pmatrix} \tag{38}$$

$$\sim \begin{pmatrix} 1 & 2 & \cdots & r \\ t_{g_1}^{[L]} & t_{g_2}^{[L]} & \cdots & t_{g_r}^{[L]} \end{pmatrix} = p_g^{[L]}, \tag{39}$$

where the degree of each permutation is equal to $r = |\mathbf{G}|/|\mathbf{H}|$. When g runs over $\mathbf{G}$, the permutation $p_g^{[L]}$ constructs a LCR of $\mathbf{G}$ modulo $\mathbf{H}$ as follows:

$$\mathbf{G}(/\mathbf{H}) = \{p_g^{[L]} \mid \forall g \in \mathbf{G}\}. \tag{40}$$

The ith components $\mathbf{H}g_i$ and $\mathbf{H}g_ig$ in equation (3) correspond to the ith components $g_i^{-1}\mathbf{H}$ and $(g_ig)^{-1}\mathbf{H}$ $(= g^{-1}g_i^{-1}\mathbf{H})$ in equation (38), respectively. When g_i moves from $i = 1$ to r, the resulting permutations $p_g^{[R]}$ $(\in (\mathbf{H}\backslash)\mathbf{G})$ and $p_{g^{-1}}^{[L]}$ $(\in \mathbf{G}(/\mathbf{H}))$ are essentially equal to each other. It follows that we obtain:

$$p_g^{[R]} = p_{g^{-1}}^{[L]}. \tag{41}$$

On the same line, the following equation can be derived:

$$p_{g^{-1}}^{[R]} = p_g^{[L]}. \tag{42}$$

These results are summarized as a theorem:

Theorem 1. The RCR $(\mathbf{H}\backslash)\mathbf{G}$ (equation (5)) and the LCR $\mathbf{G}(/\mathbf{H})$ (equation (40)) are so equivalent as to satisfy equations (41) and (42).

Example 3. This example shows a LCR $\mathbf{D}_{2d}(/\mathbf{C}_s)$ by starting from equation (11). According to equation (36), we obtain the corresponding left coset decomposition as follows:

$$\mathbf{D}_{2d} = \mathbf{C}_s + C_{2(1)}^{-1}\mathbf{C}_s + C_{2(3)}^{-1}\mathbf{C}_s + C_{2(2)}^{-1}\mathbf{C}_s \tag{43}$$

$$= \underbrace{\{1, 5\}}_{1} + \underbrace{\{2, 7\}}_{2} + \underbrace{\{4, 8\}}_{3} + \underbrace{\{3, 6\}}_{4}, \tag{44}$$

where the numbering of the symmetry operations contained in each coset is shown in figure 2. The numbering of the left cosets in equation (44) corresponds

to that of the right cosets in equation (21). Then, the following set of right cosets is obtained:

$$\mathbf{D}_{2d}/\mathbf{C}_s = \{\underbrace{\mathbf{C}_s}_{1}, \underbrace{C_{2(1)}^{-1}\mathbf{C}_s}_{2}, \underbrace{C_{2(3)}^{-1}\mathbf{C}_s}_{3}, \underbrace{C_{2(2)}^{-1}\mathbf{C}_s}_{4}\}, \tag{45}$$

where these cosets are numbered sequentially from 1 to 4. The mode of numbering should be selected in agreement with equation (45) (i.e., $C_{2(1)} \leftrightarrow C_{2(1)}^{-1}$, etc. and $g_i \leftrightarrow g_i^{-1}$ in general). The concrete form of the LCR $\mathbf{D}_{2d}(/\mathbf{C}_s)$ is calculated as follows:

$$I \sim \begin{pmatrix} 1 & 2 & 3 & 4 \\ 1 & 2 & 3 & 4 \end{pmatrix} = (1)(2)(3)(4), \tag{46}$$

$$C_{2(1)} \sim \begin{pmatrix} 1 & 2 & 3 & 4 \\ 2 & 1 & 4 & 3 \end{pmatrix} = (1\ 2)(3\ 4), \tag{47}$$

$$C_{2(2)} \sim \begin{pmatrix} 1 & 2 & 3 & 4 \\ 4 & 3 & 2 & 1 \end{pmatrix} = (1\ 4)(2\ 3), \tag{48}$$

$$C_{2(3)} \sim \begin{pmatrix} 1 & 2 & 3 & 4 \\ 3 & 4 & 1 & 2 \end{pmatrix} = (1\ 3)(2\ 4), \tag{49}$$

$$\sigma_{d(1)} \sim \begin{pmatrix} 1 & 2 & 3 & 4 \\ \bar{1} & \bar{4} & \bar{3} & \bar{2} \end{pmatrix} = \overline{(1)(3)(2\ 4)}, \tag{50}$$

$$S_4 \sim \begin{pmatrix} 1 & 2 & 3 & 4 \\ \bar{4} & \bar{1} & \bar{2} & \bar{3} \end{pmatrix} = \overline{(1\ 4\ 3\ 2)}, \tag{51}$$

$$S_4^3 \sim \begin{pmatrix} 1 & 2 & 3 & 4 \\ \bar{2} & \bar{3} & \bar{4} & \bar{1} \end{pmatrix} = \overline{(1\ 2\ 3\ 4)}, \tag{52}$$

$$\sigma_{d(2)} \sim \begin{pmatrix} 1 & 2 & 3 & 4 \\ \bar{3} & \bar{2} & \bar{1} & \bar{4} \end{pmatrix} = \overline{(1\ 3)(2)(4)}, \tag{53}$$

where an overbar represents the invertion of one chirality into an opposite chirality. The comparison of examples 2 and 3 exemplifies equations (41) and (42). □

2.2. *Marks and fixed-point vectors*

Coset representations can be characterized by a set of *marks*, which is called a Fixed Point Vector (FPV) to emphasize its geometrical or stereochemical meaning, as described in Chapter 5 of Fujita's book [12]. Thus, a mark of **K** on the RCR (**H**\)**G** or on the LCR **G**(/**H**) is the number of immobile cosets by the restriction of the RCR or LCR within the subgroup **K**. When the **K** runs over the SSG of the group **G**, the resulting marks construct a row vector, which is called a FPV. Because of the correspondence between equations (1) and equation (36), the FPV due to the RCR is equal to the FPV due to the LCR.

Example 4. In order to obtain the mark of the subgroup $\mathbf{C}_s$ on the RCR $(\mathbf{C}_s\backslash)\mathbf{D}_{2d}$, we select

$$\mathbf{C}_s = \{I, \sigma_{d(1)}\} \sim \{(1)(2)(3)(4), (1)(2)(3\ 4)\} \tag{54}$$

from the permutations of the RCR (equations (28)–(35)). The two points (i.e., 1 and 2) are immobile under $\mathbf{C}_s$ so that the mark is equal to 2. The other marks can be obtained similarly. They are aligned in the order of the SSG shown in equation (19) so as to give an FPV = (4, 0, 0, 2, 0, 0, 0, 0). This procedure is applied to all of the RCRs, each of which is obtained in accord with a subgroup listed in the SSG. By collecting the resulting FPVs as rows, we can construct a mark table (or a table of marks) as shown in table 1, which has been reported in Appendix A.8 of Fujita's book [12].

As found easily, the FPVs for respective RCRs (or LCRs) are different from each other. This means that each RCR (or LCR) is characterized by the corresponding FPV appearing as a row of a mark table. Moreover, any set of FPVs exhibits additivity to give a summed FPV.

The mark table shown in table 1 can be regarded as a square matrix $M_{\mathbf{D}_{2d}}$. Because the $M_{\mathbf{D}_{2d}}$ is a lower-triangular matrix with non-zero diagonal elements, it has the inverse matrix $(M^{-1}_{\mathbf{D}_{2d}})$. This matrix is shown as a tabular form (table 2), where the sum of each row is shown in the rightmost column for the sake of convenience. Note that the sums of non-cyclic subgroups vanish to become equal to zero. Table 2 has been reported in Appendix B.8 of Fujita's book [12].

Because of the additivity of FPVs, the multiplicity of each component FPV involved in a summed FPV can be calculated by the multiplication of the summed FPV by the inverse mark table. For example, if a summed FPV = (24, 4, 0, 2, 0, 0, 0, 0) is given, the multiplicity of each component FPV

Table 1
Mark table for $\mathbf{D}_{2d}$ [12].

RCR	LCR	$\mathbf{C}_1$	$\mathbf{C}_2$	$\mathbf{C}_2'$	$\mathbf{C}_s$	$\mathbf{S}_4$	$\mathbf{C}_{2v}$	$\mathbf{D}_2$	$\mathbf{D}_{2d}$
$(\mathbf{C}_1\backslash)\mathbf{D}_{2d}$	$\mathbf{D}_{2d}(/\mathbf{C}_1)$	8	0	0	0	0	0	0	0
$(\mathbf{C}_2\backslash)\mathbf{D}_{2d}$	$\mathbf{D}_{2d}(/\mathbf{C}_2)$	4	4	0	0	0	0	0	0
$(\mathbf{C}_2'\backslash)\mathbf{D}_{2d}$	$\mathbf{D}_{2d}(/\mathbf{C}_2')$	4	0	2	0	0	0	0	0
$(\mathbf{C}_s\backslash)\mathbf{D}_{2d}$	$\mathbf{D}_{2d}(/\mathbf{C}_s)$	4	0	0	2	0	0	0	0
$(\mathbf{S}_4\backslash)\mathbf{D}_{2d}$	$\mathbf{D}_{2d}(/\mathbf{S}_4)$	2	2	0	0	2	0	0	0
$(\mathbf{C}_{2v}\backslash)\mathbf{D}_{2d}$	$\mathbf{D}_{2d}(/\mathbf{C}_{2v})$	2	2	0	2	0	2	0	0
$(\mathbf{D}_2\backslash)\mathbf{D}_{2d}$	$\mathbf{D}_{2d}(/\mathbf{D}_2)$	2	2	2	0	0	0	2	0
$(\mathbf{D}_{2d}\backslash)\mathbf{D}_{2d}$	$\mathbf{D}_{2d}(/\mathbf{D}_{2d})$	1	1	1	1	1	1	1	1

Table 2
Inverse mark table for $\mathbf{D}_{2d}$ [12].

RCR / LCR	$(\mathbf{C}_1\backslash)$ $(/\mathbf{C}_1)$	$(\mathbf{C}_2\backslash)$ $(/\mathbf{C}_2)$	$(\mathbf{C}_2'\backslash)$ $(/\mathbf{C}_2')$	$(\mathbf{C}_s\backslash)$ $(/\mathbf{C}_s)$	$(\mathbf{S}_4\backslash)$ $(/\mathbf{S}_4)$	$(\mathbf{C}_{2v}\backslash)$ $(/\mathbf{C}_{2v})$	$(\mathbf{D}_2\backslash)$ $(/\mathbf{D}_2)$	$(\mathbf{D}_{2d}\backslash)$ $(/\mathbf{D}_{2d})$	sum
$\mathbf{C}_1$	$\frac{1}{8}$	0	0	0	0	0	0	0	$\frac{1}{8}$
$\mathbf{C}_2$	$-\frac{1}{8}$	$\frac{1}{4}$	0	0	0	0	0	0	$\frac{1}{8}$
$\mathbf{C}_2'$	$-\frac{1}{4}$	0	$\frac{1}{2}$	0	0	0	0	0	$\frac{1}{4}$
$\mathbf{C}_s$	$-\frac{1}{4}$	0	0	$\frac{1}{2}$	0	0	0	0	$\frac{1}{4}$
$\mathbf{S}_4$	0	$-\frac{1}{4}$	0	0	$\frac{1}{2}$	0	0	0	$\frac{1}{4}$
$\mathbf{C}_{2v}$	$\frac{1}{4}$	$-\frac{1}{4}$	0	$-\frac{1}{2}$	0	$\frac{1}{2}$	0	0	0
$\mathbf{D}_2$	$\frac{1}{4}$	$-\frac{1}{4}$	$-\frac{1}{2}$	0	0	0	$\frac{1}{2}$	0	0
$\mathbf{D}_{2d}$	0	$\frac{1}{2}$	0	0	$-\frac{1}{2}$	$-\frac{1}{2}$	$-\frac{1}{2}$	1	0

is calculated as follows:

$$(24, 4, 0, 2, 0, 0, 0, 0)M^{-1}_{\mathbf{D}_{2d}} = (2, 1, 0, 1, 0, 0, 0, 0, 0, 0) \tag{55}$$

the right-hand side of which shows the appearance of two $(\mathbf{C}_1\backslash)\mathbf{D}_{2d}$-rows, one $(\mathbf{C}_2\backslash)\mathbf{D}_{2d}$-row, and one $(\mathbf{C}_s\backslash)\mathbf{D}_{2d}$-row of table 1.

The mark tables and the inverse mark tables for representative point groups have been summarized in Appendices A and B of Fujita's book [12].

2.3. *Sphericities of orbits and USCI-CFs*

According to Chapter 9 of Fujita's book [12], the restriction of the RCR $(\mathbf{H}\backslash)\mathbf{G}$ within the subgroup $\mathbf{K}$ is called *the subduction of the RCR* and represented by the symbol $(\mathbf{H}\backslash)\mathbf{G} \downarrow \mathbf{K}$, which is derived from equation (3) as follows:

$$(\mathbf{H}\backslash)\mathbf{G} \downarrow \mathbf{K} = \{p_g^{[R]} | \forall g \in \mathbf{K}\}. \tag{56}$$

The resulting representation of the subgroup $\mathbf{K}$ is generally represented by the sum of RCRs of $\mathbf{K}$ as follows:

$$(\mathbf{H}\backslash)\mathbf{G} \downarrow \mathbf{K} = \sum_{\mathbf{L}} \alpha_{\mathbf{L}} (\mathbf{L}\backslash)\mathbf{K}, \tag{57}$$

where the summation is concerned with all of the subgroups $\mathbf{L}$ of $\mathbf{K}$ up to conjugacy.

Although the treatment described in Chapter 9 of Fujita's book [12] is concerned with RCRs, it can be applied to LCRs on the same line. Thus, *the subduction of the LCR* $\mathbf{G}(/\mathbf{H}) \downarrow \mathbf{K}$ is derived from equation (40) as follows:

$$\mathbf{G}(/\mathbf{H}) \downarrow \mathbf{K} = \{p_g^{[L]} | \forall g \in \mathbf{K}\}. \tag{58}$$

The resulting representation is regarded as a representation of the subgroup **K**, which is generally represented by the sum of LCRs of **K** as follows:

$$\mathbf{G}(/\mathbf{H}) \downarrow \mathbf{K} = \sum_{\mathbf{L}} \alpha_{\mathbf{L}} \mathbf{K}(/\mathbf{L}), \tag{59}$$

where the summation is concerned with all of the subgroups **L** of **K** up to conjugacy.

The symbol $\alpha_{\mathbf{L}}$ of equation (57) or (59) is a non-negative integer representing the multiplicity of each resulting RCR or LCR of **K**. Because the subduction process to **K** (equation (57) or (59)) is essentially the same as the process which has been done to calculate the mark of the RCR or the LCR by **K**, the mark is equal to the multiplicity of a one-degree RCR $(\mathbf{K}\backslash)\mathbf{K}$ or LCR $\mathbf{K}(/\mathbf{K})$. That is to say, the multiplicity $\alpha_{\mathbf{K}}$ represents the corresponding mark.

To comprehend the subductions represented by equations (57) and (59), we should add some comments on the actions of $(\mathbf{L}\backslash)\mathbf{K}$ and $\mathbf{K}(/\mathbf{L})$. Because these actions are equivalent, only the action of $(\mathbf{L}\backslash)\mathbf{K}$ will be discussed here. As a result of the subduction $(\mathbf{H}\backslash)\mathbf{G} \downarrow \mathbf{K}$ (equation (57)), there emerges a set of cosets

$$\mathrm{SC}_{\mathbf{K}} = \{\mathbf{H}g_i k \quad | \quad \forall k \in \mathbf{K}\} \tag{60}$$

by starting from the $\mathbf{H}g_i$ (tentatively fixed), where the resulting cosets are contained in the the original $\mathbf{H}\backslash\mathbf{G}$, i.e., $\mathrm{SC}_{\mathbf{K}} \subset \mathbf{H}\backslash\mathbf{G}$. Note that the set $\mathrm{SC}_{\mathbf{K}}$ may have some redundancy so as to have two or more equal cosets. Hence, let **L** be a subset of **K**, which gives a set of such equal cosets that satisfy $\mathbf{H}g_i = \mathbf{H}g_i\ell = \mathbf{H}g_i\ell'$ for any two elements ℓ and ℓ' $(\in \mathbf{L})$. Because $\mathbf{H}g_i\ell\ell' = \mathbf{H}g_i\ell' = \mathbf{H}g_i$, the subset **L** is a subgroup of **K**. Thereby, the following set of right cosets is obtained:

$$\mathbf{L}\backslash\mathbf{K} = \{\mathbf{L}k_1, \mathbf{L}k_2, \ldots, \mathbf{L}k_{|\mathbf{K}|/|\mathbf{L}|}\}, \tag{61}$$

which is governed by the RCR $(\mathbf{L}\backslash)\mathbf{K}$. By using the representatives of $\mathbf{L}\backslash\mathbf{K}$, i.e., $\{k_1(=I), k_2, \ldots, k_{|\mathbf{K}|/|\mathbf{L}|}\}$, the redundancy described above is deleted from the $\mathrm{SC}_{\mathbf{K}}$ (equation (60)) to give another set of cosets:

$$\mathrm{SC}_{\mathbf{L}\backslash\mathbf{K}} = \{\mathbf{H}g_i k_1, \mathbf{H}g_i k_2, \ldots, \mathbf{H}g_i k_{|\mathbf{K}|/|\mathbf{L}|}\}, \tag{62}$$

which is a non-redundant subset of the original $\mathbf{H}\backslash\mathbf{G}$. Because every cosets of the set $\mathrm{SC}_{\mathbf{L}\backslash\mathbf{K}}$ (equation (62)) correspond to those of the set $\mathbf{L}\backslash\mathbf{K}$ (equation (61)) in a one-to-one fashion, we can say that the set $\mathrm{SC}_{\mathbf{L}\backslash\mathbf{K}}$ (equation 62) is governed by the RCR $(\mathbf{L}\backslash)\mathbf{K}$. Because the **L** depends on the $\mathbf{H}g_i$ fixed tentatively, the procedure of generating $\mathrm{SC}_{\mathbf{L}\backslash\mathbf{K}}$ is repeated by moving $\mathbf{H}g_i$ to cover the original set $\mathbf{H}\backslash\mathbf{G}$ so as to satisfy equation (57).

The two equations (57) and (59) are essentially equivalent so as to select common multiplicities (i.e., $\alpha_{\mathbf{L}}$). The calculation of such multiplicities has once

been discussed in Chapter 9 of Fujita's book [12]. The subduction results for representative point groups have been summarized in Appendix C of the same book [12].

Each CR (RCR $(\mathbf{H}\backslash)\mathbf{G}$ or LCR $\mathbf{G}(/\mathbf{H})$) is characterized as being homospheric, enantiospheric, or hemispheric according to the chirality/achirality of the relevant groups, as listed in table 3 [12, 14]. Thereby, the corresponding sphericity index is defined as found in table 3, i.e., a_d for a homospheric CR, c_d for an enantiospheric CR, or b_d for a hemispheric CR. Because each CR governs an orbit (equivalence class) of objects (atoms, proligands, ligands, etc.), we can say that the orbit is also characterized by the sphericity and by the sphericity index.

Because each RCR appearing on the right-hand side of equation (57) or each LCR appearing on the right-hand side of equation (59) is also characterized by its sphericity index with respect to **K** (and its subgroup **L**), the subductions (equations (57) and (59)) can be characterized by a common product of sphericity indices. According to Chapter 19 of Fujita's book [12], this product is called *a unit subduced cycle index with chirality fittingness* (USCI-CF).

By moving **K** over the SSG of **G**, the subductions represented by equations (57) or (59) construct a set of USCI-CFs, which characterizes the RCR $((\mathbf{H}\backslash)\mathbf{G})$ or at the same time the LCR $(\mathbf{G}(/\mathbf{H}))$. When the **H** of the RCR or of the LCR is moved over the SSG of **G**, we can obtain *a USCI-CF table*, each row of which is composed of such a set of USCI-CFs. The USCI-CF tables for representative point groups have been summarized in Appendix E of Fujita's book [12].

Example 5. The $\mathbf{C}_s$-restriction described in example 4 corresponds to the subduction of the RCR $(\mathbf{C}_s\backslash)\mathbf{D}_{2d}$ by the subgroup $\mathbf{C}_s$, i.e., $(\mathbf{C}_s\backslash)\mathbf{D}_{2d} \downarrow \mathbf{C}_s$, The result shown on the right-hand side of equation (54) indicates that the original orbit $\{1, 2, 3, 4\}$ governed by the RCR $(\mathbf{C}_s\backslash)\mathbf{D}_{2d}$ is divided into three orbits (suborbits), i.e., $\{1\}$ governed by $(\mathbf{C}_s\backslash)\mathbf{C}_s$, $\{2\}$ governed by $(\mathbf{C}_s\backslash)\mathbf{C}_s$, and $\{3, 4\}$ governed by $(\mathbf{C}_1\backslash)\mathbf{C}_s$. According to equation (57), the present result is represented by the following equation:

$$(\mathbf{C}_s\backslash)\mathbf{D}_{2d} \downarrow \mathbf{C}_s = 2(\mathbf{C}_s\backslash)\mathbf{C}_s + (\mathbf{C}_1\backslash)\mathbf{C}_s. \tag{63}$$

Table 3
Sphericities and sphericity indices for an RCR $(\mathbf{H}\backslash)\mathbf{G}$ or an LCR $\mathbf{G}(/\mathbf{H})$ [14].

Global symmetry (**G**)	Local symmetry (**H**)	Sphericity	Sphericity index (where $d = \lvert\mathbf{G}\rvert/\lvert\mathbf{H}\rvert$)
Achiral	Achiral	Homospheric	a_d
Achiral	Chiral	Enantiospheric	c_d
Chiral	Chiral	Hemispheric	b_d

The RCRs appearing on the right-hand side of equation (63) are characterized by the respective sphericity indices, a_1 (twice) and c_2, because of the criteria shown in table 3, so that the subduction shown in equation (63) is characterized by a USCI-CF as the product of the sphericity indices, i.e., $a_1^2 c_2$. Obviously, the mark 2 obtained in example 4 corresponds to the power 2 of the sphericity index a_1, which is assigned to the immobile points {1} and {2} under $\mathbf{C}_s$ (cf. equation (54)).

This procedure is repeated by moving the subgroup $\mathbf{K}$ over the SSG of $\mathbf{D}_{2d}$ (equation (19)) so as to give the corresponding set of USCI-CFs:

$$\{b_1^4, b_2^2, b_2^2, a_1^2 c_2, c_4, a_2^2, b_4, a_4\}. \tag{64}$$

Obviously, the collection of the powers of one-cycles (a_1 and b_1) gives the corresponding FPV, i.e., (4, 0, 0, 2, 0, 0, 0, 0), which appears as the $(\mathbf{C}_s\backslash)\mathbf{D}_{2d}$-row (or $\mathbf{D}_{2d}(/\mathbf{C}_s)$-row) in table 1. The formal row vector represented by equation (64) is used to construct the $(\mathbf{C}_s\backslash)\mathbf{D}_{2d}$-row (or the $\mathbf{D}_{2d}(/\mathbf{C}_s)$-row) of the USCI-CF table shown in table 4, which is cited from Appendix E.8 of Fujita's book [12].

The sums at the bottom of table 4 ($\sum_{i=1}^{s} \overline{m}_{ji}$) are adopted from the rightmost column of table 2. They are useful to show the relationship between the USCI approach and Fujita's proligand method [35–37], although the details of the relationship will be discussed elsewhere.

3. Definitions of mandalas

3.1. Regular representations and regular bodies

3.1.1. The numbering of regular bodies

An extreme case of RCRs in which $\mathbf{H}$ is an identity group (i.e., $\mathbf{H} = \mathbf{C}_1 = \{I\}$) is called *a right regular representation* (RRR), which is represented by the

Table 4
USCI-CF table for $\mathbf{D}_{2d}$ [12].

		$\downarrow\mathbf{C}_1$	$\downarrow\mathbf{C}_2$	$\downarrow\mathbf{C}_2'$	$\downarrow\mathbf{C}_s$	$\downarrow\mathbf{S}_4$	$\downarrow\mathbf{C}_{2v}$	$\downarrow\mathbf{D}_2$	$\downarrow\mathbf{D}_{2d}$
$(\mathbf{C}_1\backslash)\mathbf{D}_{2d}$	$\mathbf{D}_{2d}(/\mathbf{C}_1)$	b_1^8	b_2^4	b_2^4	c_2^4	c_4^2	c_4^2	b_4^2	c_8
$(\mathbf{C}_2\backslash)\mathbf{D}_{2d}$	$\mathbf{D}_{2d}(/\mathbf{C}_2)$	b_1^4	b_1^4	b_2^2	c_2^2	c_2^2	c_2^2	b_2^2	c_4
$(\mathbf{C}_2'\backslash)\mathbf{D}_{2d}$	$\mathbf{D}_{2d}(/\mathbf{C}_2')$	b_1^4	b_2^2	$b_1^2 b_2$	c_2^2	c_4	c_4	b_2^2	c_4
$(\mathbf{C}_s\backslash)\mathbf{D}_{2d}$	$\mathbf{D}_{2d}(/\mathbf{C}_s)$	b_1^4	b_2^2	b_2^2	$a_1^2 c_2$	c_4	a_2^2	b_4	a_4
$(\mathbf{S}_4\backslash)\mathbf{D}_{2d}$	$\mathbf{D}_{2d}(/\mathbf{S}_4)$	b_1^2	b_1^2	b_2	c_2	a_1^2	c_2	b_2	a_2
$(\mathbf{C}_{2v}\backslash)\mathbf{D}_{2d}$	$\mathbf{D}_{2d}(/\mathbf{C}_{2v})$	b_1^2	b_1^2	b_2	a_1^2	c_2	a_1^2	b_2	a_2
$(\mathbf{D}_2\backslash)\mathbf{D}_{2d}$	$\mathbf{D}_{2d}(/\mathbf{D}_2)$	b_1^2	b_1^2	b_1^2	c_2	c_2	c_2	b_1^2	c_2
$(\mathbf{D}_{2d}\backslash)\mathbf{D}_{2d}$	$\mathbf{D}_{2d}(/\mathbf{D}_{2d})$	b_1	b_1	b_1	a_1	a_1	a_1	b_1	a_1
	$\sum_{i=1}^{s} \overline{m}_{ji}$	1/8	1/8	1/4	1/4	1/4	0	0	0

symbol $(\mathbf{C}_1\backslash)\mathbf{G}$. The RRR governs the following set obtained by replacing $\mathbf{H}$ by $\mathbf{C}_1$ in equation (2), i.e.,

$$\mathbf{C}_1\backslash\mathbf{G} = \{\underbrace{g_1}_{1}, \underbrace{g_2}_{2}, \ldots, \underbrace{g_n}_{n}\}, \tag{65}$$

where we place $g_1 = I$ and $n = |\mathbf{G}|$. The set $\mathbf{C}_1\backslash\mathbf{G}$ is an ordered set that is identical with the group $\mathbf{G}$ itself. Although there are $n!$ permutations for numbering the set, an arbitrary one can be selected as a reference numbering without losing generality.

Example 6. The concrete form of the RRR $(\mathbf{C}_1\backslash)\mathbf{D}_{2d}$ is obtained by selecting each column of the multiplication table (figure 2), i.e.,

$$I \sim \begin{pmatrix} 1&2&3&4&5&6&7&8 \\ 1&2&3&4&5&6&7&8 \end{pmatrix} = (1)(2)(3)(4)(5)(6)(7)(8), \tag{66}$$

$$C_{2(1)} \sim \begin{pmatrix} 1&2&3&4&5&6&7&8 \\ 2&1&4&3&6&5&8&7 \end{pmatrix} = (1\ 2)(3\ 4)(5\ 6)(7\ 8), \tag{67}$$

$$C_{2(2)} \sim \begin{pmatrix} 1&2&3&4&5&6&7&8 \\ 3&4&1&2&7&8&5&6 \end{pmatrix} = (1\ 3)(2\ 4)(5\ 7)(6\ 8), \tag{68}$$

$$C_{2(3)} \sim \begin{pmatrix} 1&2&3&4&5&6&7&8 \\ 4&3&2&1&8&7&6&5 \end{pmatrix} = (1\ 4)(2\ 3)(5\ 8)(6\ 7), \tag{69}$$

$$\sigma_{d(1)} \sim \begin{pmatrix} 1&2&3&4&5&6&7&8 \\ \overline{5}&\overline{7}&\overline{6}&\overline{8}&\overline{1}&\overline{3}&\overline{2}&\overline{4} \end{pmatrix} = \overline{(1\ 5)(2\ 7)(3\ 6)(4\ 8)}, \tag{70}$$

$$S_4 \sim \begin{pmatrix} 1&2&3&4&5&6&7&8 \\ \overline{6}&\overline{8}&\overline{5}&\overline{7}&\overline{2}&\overline{4}&\overline{1}&\overline{3} \end{pmatrix} = \overline{(1\ 6\ 4\ 7)(2\ 8\ 3\ 5)}, \tag{71}$$

$$S_4^3 \sim \begin{pmatrix} 1&2&3&4&5&6&7&8 \\ \overline{7}&\overline{5}&\overline{8}&\overline{6}&\overline{3}&\overline{1}&\overline{4}&\overline{2} \end{pmatrix} = \overline{(1\ 7\ 4\ 6)(2\ 5\ 3\ 8)}, \tag{72}$$

$$\sigma_{d(2)} \sim \begin{pmatrix} 1&2&3&4&5&6&7&8 \\ \overline{8}&\overline{6}&\overline{7}&\overline{5}&\overline{4}&\overline{2}&\overline{3}&\overline{1} \end{pmatrix} = \overline{(1\ 8)(2\ 6)(3\ 7)(4\ 5)}, \tag{73}$$

where an overbar represents the invertion of one chirality into an opposite chirality.

According to Chapter 7 of Fujita's book [12], a regular body of $\mathbf{G}$-symmetry is defined as a three-dimensional objects having $|\mathbf{G}|$ equivalent positions that are governed by an RRR $(\mathbf{C}_1\backslash)\mathbf{G}$. The numbering of the positions is selected in accord with the numbering of elements shown in equation (65). Thus, the element g_i $(i = 1, 2, \ldots, n)$ acts on the ith position of the regular body so as to shift it into the first position selected arbitrarily as a reference $(g_1 = I)$. This numbering, which is called *a reference numbering*, assures the one-to-one correspondence between each element of $\mathbf{G}$ (equation (65)) and each position of the resulting regular body.

It should be noted here that a regular body can be interpreted in two ways. One way is to distinguish the $|\mathbf{G}|$ equivalent positions in accord with distinct modes of numbering so that the set of $|\mathbf{G}|$ equivalent positions governed by the RRR $(\mathbf{C}_1\backslash)\mathbf{G}$. The other way is to transform the regular body into $|\mathbf{G}|$ regular bodies, where the set of the resulting equivalent regular bodies is regarded as constructing a one-membered orbit governed by LCR $\mathbf{G}(/\mathbf{G})$.

Example 7. A regular body (**1′**) for $\mathbf{D}_{2d}$ is shown in figure 3, where two cyclopropane rings attach to the terminal carbons of an allene skeleton in a perpendicular fashion so as to maintain the $\mathbf{D}_{2d}$-symmetry (cf. figure 1). For the sake of convenience, the topview (**1**) is used in the following discussions. Although this regular body has once been discussed in Chapter 7 of Fujita's book [12], the mode of numbering is changed to meet the numbering adopted in equation (65) and figure 2. Thereby, the RRR shown in equations (66)–(73) controls the symmetry of the resulting regular body (**1**).

Although the numbering of the vertices can be selected arbitrarily, it should be consistent with the numbering of the symmetry operations shown in the multiplication table (figure 2). In other words, once we select the numbering shown in figure 2, the numbering of the vertices is decided, as indicated in the caption of figure 3.

In accord with the RRR defined above (equation (65)), a left regular representation (LRR), $\mathbf{G}(/\mathbf{C}_1)$, is obtained so as to govern the following set obtained by replacing $\mathbf{H}$ by $\mathbf{C}_1$ in equation (37), i.e.,

$$\mathbf{G}/\mathbf{C}_1 = \{\underbrace{g_1^{-1}}_{t_1}, \underbrace{g_2^{-1}}_{t_2}, \ldots, \underbrace{g_n^{-1}}_{t_n}\}, \tag{74}$$

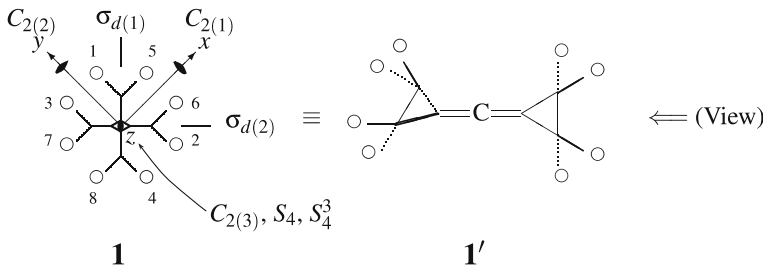

Figure 3. Regular body for $\mathbf{D}_{2d}$. The position 1 operated by I [1] is permuted into the position 1; the position 2 operated by $C_{2(1)}$ [2] into the position 1; the position 3 operated by $C_{2(2)}$ [3] into the position 1; the position 4 operated by $C_{2(3)}$ [4] into the position 1; the position 5 operated by $\sigma_{d(1)}$ [5] into the position 1; the position 6 operated by S_4 [6] into the position 1; the position 7 operated by S_4^3 [7] into the position 1; and the position 4 operated by $\sigma_{d(2)}$ [8] into the position 1. The number in each pair of parentheses represents the correspondence to the multiplication table shown in figure 2.

where we place $g_1^{-1} = I, t_1 = 1$, and $n = |\mathbf{G}|$. The set $\mathbf{G}/\mathbf{C}_1$ is an ordered set, which is determined in accord with the LRR shown in equation (74). Note that the RRR shown in equation (65) and the LRR shown in equation (74) are correlated to each other by the numbering of their elements.

On the same line as the reference numbering of the regular body, another mode of numbering of the regular body of **G**-symmetry can be adopted on the basis of the LRR $\mathbf{G}(/\mathbf{C}_1)$ shown in equation (74). This numbering is called *the inverse* of the reference numbering. The discrimination between the reference numbering and its inverse is an essential point to discuss the symmetrical properties of regular bodies and mandalas described below.

Example 8. A regular body with the inverse numbering ($\widetilde{\mathbf{1}}$) for $\mathbf{D}_{2d}$ is shown in figure 4, where the mode of numbering is changed to meet the one adopted in equation (74).

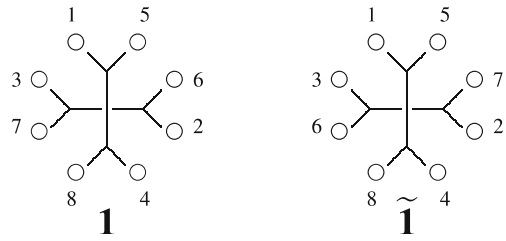

Figure 4. Regular body with a reference numbering (**1**) and with the inverse numbering ($\widetilde{\mathbf{1}}$).

Note that the inverse numbering is selected to transform the RRR $(\mathbf{C}_1\backslash)\mathbf{D}_{2d}$ (equal to equation (11)) into the LRR $\mathbf{D}_{2d}/\mathbf{C}_1$ as follows:

$$\begin{aligned}\mathbf{D}_{2d}/\mathbf{C}_1 &= \{\underbrace{I^{-1}}_{1}, \underbrace{C_{2(1)}^{-1}}_{2}, \underbrace{C_{2(2)}^{-1}}_{3}, \underbrace{C_{2(3)}^{-1}}_{4}; \underbrace{\sigma_{d(1)}^{-1}}_{5}, \underbrace{S_4^{-1}}_{6}, \underbrace{S_4^{-3}}_{7}, \underbrace{\sigma_{d(2)}^{-1}}_{8}\} \\ &= \{\underbrace{I}_{1}, \underbrace{C_{2(1)}}_{2}, \underbrace{C_{2(2)}}_{3}, \underbrace{C_{2(3)}}_{4}; \underbrace{\sigma_{d(1)}}_{5}, \underbrace{S_4^3}_{6}, \underbrace{S_4}_{7}, \underbrace{\sigma_{d(2)}}_{8}\}. \end{aligned} \tag{75}$$

The exchange between S_4 and S_4^3 for equations (11) and (75) corresponds to the exchange between positions 6 and 7 for the reference numbering (**1**) and the inverse numbering ($\widetilde{\mathbf{1}}$).

3.1.2. Segmentation of regular bodies

The RCR shown in equation (5) causes the partition of the positions contained in the corresponding regular body with the reference numbering. The resulting $|\mathbf{G}|/|\mathbf{H}|$ sets of positions are called **H**-*segments*, which construct an

orbit governed by the RCR (equation (5)). Because each right coset $\mathbf{H}g_i$ governed by the RCR satisfies the relationship $\mathbf{H}g_i(g_i^{-1}\mathbf{H}g_i) = \mathbf{H}g_i$, it is fixed on the action of $g_i^{-1}\mathbf{H}g_i$, which is conjugate to $\mathbf{H}$. This means that each $\mathbf{H}$-segment belongs to either one of the conjugate subgroups $g_i^{-1}\mathbf{H}g_i$ $(i = 1, 2, \ldots, r)$. In other words, the conjugate subgroups $g_i^{-1}\mathbf{H}g_i$ are equalize to $\mathbf{H}$ under $\mathbf{G}$ so that the $\mathbf{H}$ is regarded as the local symmetry of the segments and the $\mathbf{G}$ is regarded as the global symmetry of the regular body. The resulting mode of partition (segmentation) is called *a segmentation pattern*. It should be noted that the $\mathbf{H}$-segmentation maintains the $\mathbf{G}$-symmetry of the original regular body and that the regular body itself can be regarded as $\mathbf{C}_1$-segmentation, which is an extreme case of the $\mathbf{H}$-segmentation.

Example 9. In terms of equation (21), the eight positions contained in the regular body (**1**) are partitioned into four sets, as encircled by ovals (**2** in figure 5). The resulting set of segments $\mathcal{A} = \{\mathcal{A}_1, \mathcal{A}_2, \mathcal{A}_3, \mathcal{A}_4\}$ corresponds to the set of right cosets (equation (22)) so that the set $\mathcal{A}$ is governed by the RCR shown in equations (28)–(35).

As for $\mathbf{C}'_s$, another segmentation pattern (**3**) is obtained by considering the following right coset decomposition:

$$\mathbf{D}_{2d} = \mathbf{C}'_s + \mathbf{C}'_s C_{2(1)} + \mathbf{C}'_s C_{2(3)} + \mathbf{C}'_s C_{2(2)} \tag{76}$$

$$= \underbrace{\{1, 8\}}_{4} + \underbrace{\{2, 7\}}_{3} + \underbrace{\{4, 5\}}_{2} + \underbrace{\{3, 6\}}_{1}, \tag{77}$$

where the numbering of the symmetry operations contained in each coset is shown in figure (2). The set of segments is represented as $\mathcal{A}' = \{\mathcal{A}'_4, \mathcal{A}'_3, \mathcal{A}'_2, \mathcal{A}'_1\}$ (figure 5) in accord with the numbering shown in equation (77). Thereby, the set $\mathcal{A}'$ is governed by the RCR shown in equations (28)–(35). It should be noted that the segmentation patterns shown in figure 5 maintain the $\mathbf{D}_{2d}$-symmetry of the regular body.

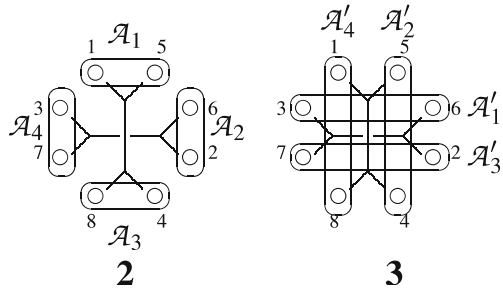

Figure 5. Segmentation patterns to generate orbits of $\mathbf{C}_s$-segments in the regular body (**1**) for illustrating the RCR $(\mathbf{C}_s \backslash) \mathbf{D}_{2d}$. Each segment encircled by an oval is called a $\mathbf{C}_s$-segment because it is fixed (stabilized) on the action of $\mathbf{C}_s$ (or its conjugate subgroup $\mathbf{C}'_s$).

The segmentation process described here has been discussed in terms of blocks and local symmetries in Chapter 7 of Fujita's book [12]. The term "blocks" is replaced here by a more chemical term *segments*.

Example 10. Chemically speaking, the set of segments $\mathcal{A} = \{\mathcal{A}_1, \mathcal{A}_2, \mathcal{A}_3, \mathcal{A}_4\}$ in **2** should be replaced by the set of substitution positions so as to give a reduced regular body (**4**), which has a more concrete chemical meaning as shown in figure 6. The reduced regular body (**4**) as a secondary skeleton is further substituted by atoms or ligands (or proligands in general). For example, the positions of **4** are replaced by hydrogen atoms to give an allene molecule. It should be emphasized that the set of segments $\mathcal{A} = \{\mathcal{A}_1, \mathcal{A}_2, \mathcal{A}_3, \mathcal{A}_4\}$ in **2**, the set of positions $\{1, 2, 3, 4\}$ in **4**, and the set of hydrogens $\{H_1, H_2, H_3, H_4\}$ in **5** are all governed by the same RCR $(\mathbf{C}_s\backslash)\mathbf{D}_{2d}$, the concrete form of which is shown in equations (28)–(35).

Reversely speaking, the symmetrical properties of allene (**5**) can be discussed by using the segmented regular body (**2**) through the reduced regular body (**4**). □

3.1.3. Subduction of regular representations

The subduction of the RRR is a special case of the subduction of RCRs (equation (56)) as follows:

$$(\mathbf{C}_1\backslash)\mathbf{G} \downarrow \mathbf{K} = \{p_g^{[R]} \mid \forall g \in \mathbf{K}\}. \tag{78}$$

This subduction disturbs the transitivity of the original RRR so as to generate $|\mathbf{G}|/|\mathbf{K}|$ orbits, each of which is governed distinctly by an RRR of **K**. This process is expressed as follows:

$$(\mathbf{C}_1\backslash)\mathbf{G} \downarrow \mathbf{K} = \frac{|\mathbf{G}|}{|\mathbf{K}|}(\mathbf{C}_1\backslash)\mathbf{K} \tag{79}$$

according to equation (7.3) described in Chapter 7 of Fujita's book [12]. The result shown in equation (79) causes the desymmetrization of the corresponding

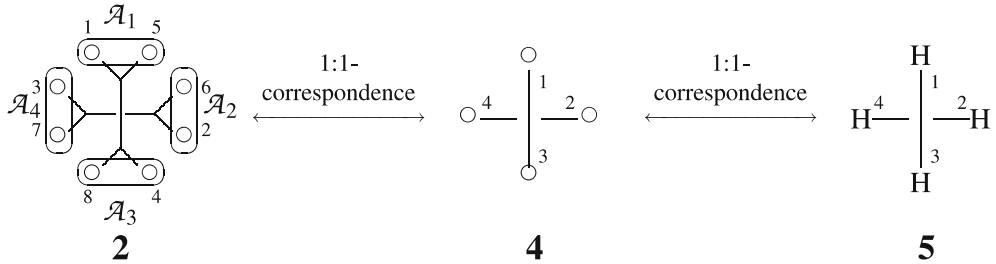

Figure 6. Derivation from a segmented regular body (**2**) to give a reduced regular body (**4**) and a molecule (**5**).

regular body so that its positions are partitioned into $|\mathbf{G}|/|\mathbf{K}|$ sets of equivalent positions under $\mathbf{K}$, where each of the sets (i.e., orbits) is governed by $(\mathbf{C}_1\backslash)\mathbf{K}$. The resulting mode of partition is called *a subduction pattern*. Obviously, equation (79) is an extreme case of equation (57), in which there emerge $|\mathbf{G}|/|\mathbf{K}|$ of regular representations of one kind.

Let us consider the relationship between the subduction $(\mathbf{C}_1\backslash)\mathbf{G} \downarrow \mathbf{H}$ and the left coset decomposition $\mathbf{G}/\mathbf{H}$ (equation (37)). When the reference numbering (equation (65)) is taken into consideration, the process of selecting $(\mathbf{C}_1\backslash)\mathbf{G} \downarrow \mathbf{H}$ is regarded as the construction of $\mathbf{C}_1 g_i g$ ($g \in \mathbf{H}$), i.e., the selection of left cosets $g_i\mathbf{H}$. Although each $g_i\mathbf{H}$ is a left coset, their numbering is in accord with the reference numbering (equation (65)). This situation is illustrated by the following example.

Example 11. We select $\mathbf{C}_s$ (equation (17)) as $\mathbf{K}$ according to equation (78). From the eight permutation contained in the RRR $(\mathbf{C}_1\backslash)\mathbf{D}_{2d}$ (equations (66)–(73)), the subduction $(\mathbf{C}_1\backslash)\mathbf{D}_{2d} \downarrow \mathbf{C}_s$ is accomplished by selecting equation (66) ($\sim I$) and equation (70) ($\sim \sigma_{d(1)}$). As a result, the transitive set of eight positions in the regular body are partitioned into four sets, i.e., $\{1, 5\}$, $\{2, 7\}$, $\{3, 6\}$, and $\{4, 8\}$ as shown in **6** (figure 7). This result is expressed as follows by applying equation (79) to this case:

$$(\mathbf{C}_1\backslash)\mathbf{D}_{2d} \downarrow \mathbf{C}_s = 4(\mathbf{C}_1\backslash)\mathbf{C}_s. \tag{80}$$

Hence, each of the four sets, i.e., $\{1, 5\}$, $\{2, 7\}$, $\{3, 6\}$, or $\{4, 8\}$, is governed by the RCR $(\mathbf{C}_1\backslash)\mathbf{C}_s$. Because these sets appear in equation (44), the subduction $(\mathbf{C}_1\backslash)\mathbf{D}_{2d} \downarrow \mathbf{C}_s$ is related to the left coset decomposition shown in equation (43).

It should be noted the subduction pattern (**6**) shown in figure 7 restricts the symmetry of the regular body within $\mathbf{C}_s$. The subduction pattern shown in **6** has a more concrete chemical meaning. For example, one of the $\mathbf{C}_s$-segments in **6**, e.g., $\{1, 5\}$, is replaced by solid circles so as to give a transformula **7**, which models the $\mathbf{C}_s$-symmetry of a (pro)molecule. Thus the resulting transformula (**7**)

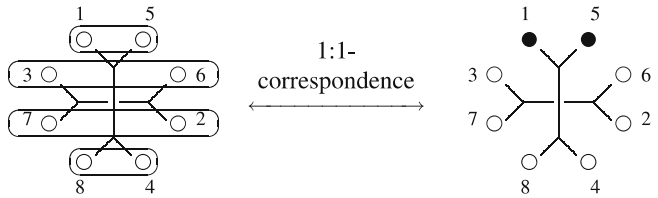

6 **7**

Figure 7. Subduction pattern generated by the subduction of RRR $(\mathbf{C}_1\backslash)\mathbf{D}_{2d}$ into $\mathbf{C}_s$. Each set encircled by an oval is regarded as a regular body of $\mathbf{C}_s$-symmetry after it is fixed (stabilized) on the action of $\mathbf{C}_s$.

belongs to the $\mathbf{C}_s$-symmetry so that each of the four sets, i.e., {1, 5}, {2, 7}, {3, 6}, or {4, 8}, is governed by the RCR $(\mathbf{C}_1\backslash)\mathbf{C}_s$. Although oval symbols are omitted in **7**, it is easy to recognize that the eight positions of the **7** are partitioned into the four sets, i.e., {1, 5}, {2, 7}, {3, 6}, and {4, 8}. For the sake of convenience, the term *transformulas* is used to designate regular bodies modified by any transformation processes such as subduction, segmentation, etc. □

Let us consider one of the $\mathbf{C}_s$-segments, e.g., {1, 5} in **2** or {3, 6} in **3**, which is regarded as exhibiting the local symmetry $\mathbf{C}_s$ in example 9. The same segment {1, 5} or {3, 6} is fixed under the subduction to $\mathbf{C}_s$, as shown in **6** of example 11. The comparison between examples 9 and 11 provides us with a new viewpoint of stereochemistry and stereoisomerism. This point will be discussed after the introduction of a new concept *mandala*.

4. Mandalas as nested regular bodies

4.1. Definition

To go on further discussions, we shall compare example 9 with example 11 in detail. This comparison reveals the relationship between the subduction $(\mathbf{C}_1\backslash)\mathbf{G} \downarrow \mathbf{H}$ and the left coset decomposition $\mathbf{G}/\mathbf{H}$ (equation (37)) so as to introduce the concept of *mandala*.

Example 12. As found in example 9, the segmentation patterns shown in figure 5 maintain the $\mathbf{D}_{2d}$-symmetry of the regular body (**1**). This feature is more clearly demonstrated by the action of the operations of $\mathbf{D}_{2d}$ on the segmented regular body (**2**), as shown in figure 8. This figure can be interpreted that the operations of $\mathbf{D}_{2d}$ act on the regular body (**1**) to produce a set of functions, $\mathcal{G}_1^*=\{f_1, f_2, f_3, f_4, f_5, f_6, f_7, f_8\}$, on which the segmentation pattern (**5**) is superposed.

Because the eight transformulas (segmented regular bodies: f_1–f_8) are identical if the numbering is omitted, they are surrounded in the box shown in figure 8. This means that the set $\mathcal{G}_1^*=\{f_1, f_2, f_3, f_4, f_5, f_6, f_7, f_8\}$ is transformed into itself under the action of $\mathbf{D}_{2d}$ so as to generate a one-membered orbit $\mathcal{G}^*=\{\mathcal{G}_1^*\}$ governed by the LCR $\mathbf{D}_{2d}(/\mathbf{D}_{2d})$. As a result, the set of segments $\{\mathcal{A}_1, \mathcal{A}_2, \mathcal{A}_3, \mathcal{A}_4\}$ is governed by the RCR $(\mathbf{C}_s\backslash)\mathbf{D}_{2d}$. The global symmetry $\mathbf{D}_{2d}$ of the RCR $(\mathbf{C}_s\backslash)\underline{\mathbf{D}_{2d}}$ corresponds to the local symmetry $\mathbf{D}_{2d}$ of the LCR $\mathbf{D}_{2d}(/\underline{\mathbf{D}_{2d}})$. □

Example 13. As found in example 11, the subduction pattern (**6**) shown in figure 7 does not maintain the $\mathbf{D}_{2d}$-symmetry of the regular body (**1**), where the subduction pattern (**6**) is fixed under $\mathbf{C}_s = \{I, \sigma_{d(1)}\}$. This feature is more clearly

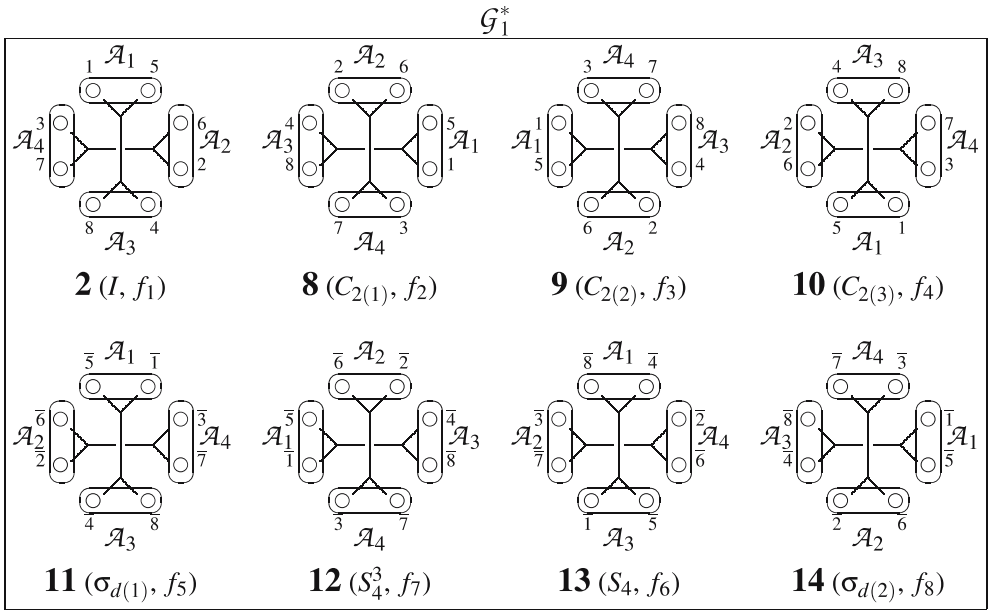

Figure 8. Eight segmented regular bodies (f_1–f_8) derived from the $\mathbf{C}_s$-segmentation pattern (**2**) under $\mathbf{D}_{2d}$. They represent the maintenance of the $\mathbf{D}_{2d}$-symmetry for the regular body so that the set of the eight segmented regular bodies (f_1–f_8) constructs a one-membered orbit governed by the LCR $\mathbf{D}_{2d}(/\mathbf{D}_{2d})$.

demonstrated by the action of the operations of $\mathbf{D}_{2d}$ on the subduction pattern (**6**), as shown in figure 9. It should be noted that **19** (S_4^3, f_7) and **20** (S_4, f_6) are placed to pair with **15** ($C_{2(1)}$, f_2) and **16** ($C_{2(2)}$, f_3), respectively, in order to be fixed under $\mathbf{C}_s$ (or its conjugate subgroup $\mathbf{C}_s'$). Thus the resulting eight transformulas (subduced regular bodies, f_1–f_8) are divided into four sets, i.e., $\mathcal{A}_1^* = \{f_1, f_5\}, \mathcal{A}_2^* = \{f_2, f_7\}, \mathcal{A}_4^* = \{f_3, f_6\}$, and $\mathcal{A}_3^* = \{f_4, f_8\}$, which are called *assemblies* as defined below. As a result, the assemblies of subduced regular bodies construct an orbit, i.e. $\mathcal{A}^* = \{\mathcal{A}_1^*, \mathcal{A}_2^*, \mathcal{A}_4^*, \mathcal{A}_3^*\}$, which is governed by LCR $\mathbf{D}_{2d}(/\mathbf{C}_s)$. Accordingly, each set of divided positions in each subduced regular body, i.e., $\{1, 5\}, \{3, 6\}, \{2, 7\}$, or $\{4, 8\}$, is governed by the RCR $(\mathbf{C}_1\backslash)\mathbf{C}_s$. The global symmetry $\mathbf{C}_s$ of the RCR $(\mathbf{C}_1\backslash)\underline{\mathbf{C}_s}$ corresponds to the local symmetry $\mathbf{C}_s$ of the LCR $\mathbf{D}_{2d}(/\underline{\mathbf{C}_s})$. □

To integrate figure 8 (the RCR $(\mathbf{C}_s\backslash)\underline{\mathbf{D}_{2d}}$ vs. the LCR $\mathbf{D}_{2d}(/\underline{\mathbf{D}_{2d}})$) and figure 9 (the RCR $(\mathbf{C}_1\backslash)\underline{\mathbf{C}_s}$ versus the LCR $\mathbf{D}_{2d}(/\underline{\mathbf{C}_s})$), an extreme case (the RCR $(\mathbf{C}_1\backslash)\underline{\mathbf{D}_{2d}}$ versus the LCR $\mathbf{D}_{2d}(/\underline{\mathbf{D}_{2d}})$) should be examined. Hence, a *mandala* is defined as a nested regular body constructed as follows:

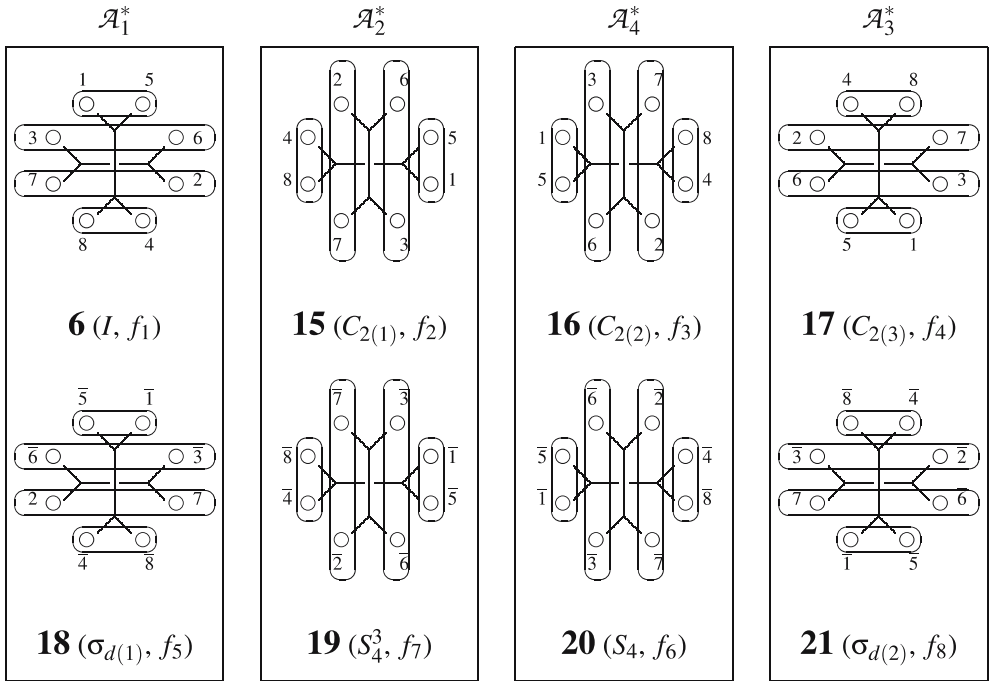

Figure 9. Eight subduced regular bodies derived from the $\mathbf{C}_s$-subduction pattern (**6**) under $\mathbf{D}_{2d}$. They represent the reduction of the $\mathbf{D}_{2d}$-symmetry for the regular body into the $\mathbf{C}_s$-symmetry for each subduced regular body. As a result, the assemblies of subduced regular bodies, $\mathcal{A}_1^* = \{f_1, f_5\}$, $\mathcal{A}_2^* = \{f_2, f_7\}$, $\mathcal{A}_4^* = \{f_3, f_6\}$, and $\mathcal{A}_3^* = \{f_4, f_8\}$, construct an orbit governed by LCR $\mathbf{D}_{2d}(/\mathbf{C}_s)$. Accordingly, each set of divided positions in each subduced regular body, i.e., {1, 5}, {3, 6}, {2, 7}, or {4, 8}, is governed by the RCR $(\mathbf{C}_1\backslash)\mathbf{C}_s$.

Definition 1. Suppose that a regular body is given, where the positions of the regular body are governed by an RRR $(\mathbf{C}_1\backslash)\mathbf{G}$ (cf. 65). Then, $|\mathbf{G}|$ of the permuted regular bodies f_1–$f_{|\mathbf{G}|}$, which are generated from the regular body by the permutations due to the group $\mathbf{G}$, are placed on the vertices of a hypothetical regular body in accord with the LRR $\mathbf{G}(/\mathbf{C}_1)$ (cf. 74) corresponding to the RRR. The resulting diagram is called *a mandala* of the group $\mathbf{G}$. The resulting mandala should be regarded as consisting of a one-membered orbit, where the regular bodies construct a one-membered orbit governed by the LCR $\mathbf{G}(/\mathbf{G})$.

It should be noted that the numbering of the original regular body obeys the reference numbering exemplified for $\mathbf{D}_{2d}$ in example 7 and that the numbering of the mandala obeys the inverse numbering exemplified in example 8.

Example 14. The transformulas (i.e., permuted regular bodies, f_1–f_8) generated on the action of $\mathbf{D}_{2d}$ are placed on the vertices of a hypothetical regular body, as shown in figure 10. The alignment of the transformulas are in agreement with the

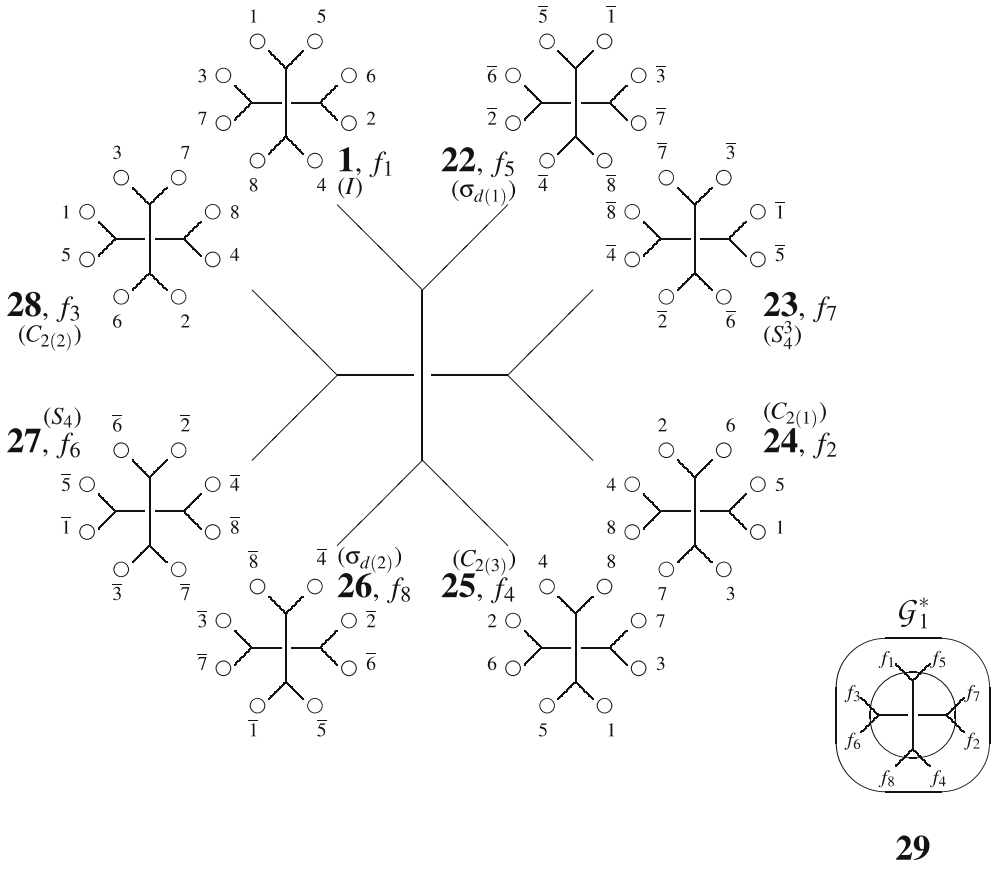

Figure 10. Mandala (a nested regular body) containing eight transformulas (f_1–f_8) at its vertices. The alignment shown in this diagram corresponds to the right diagram shown in figure 4. On the other hand, the alignment of eight positions in each regular body corresponds to the left diagram shown in figure 4. The full expression of the mandala is simplified into **29**.

right diagram ($\widetilde{\mathbf{1}}$) shown in figure 4, while the alignment of the positions of the inner regular body adopts that of the left diagram (**1**). For the sake of convenience, the full expression of the mandala (figure 10) is simplified into **29**.

Suppose that the reference regular body (**1**) is regarded as a $\mathbf{C}_1$-segmented one. Then, the eight positions of the regular body (**1**) are considered to construct an eight-membered orbit governed by $(\mathbf{C}_1\backslash)\mathbf{D}_{2d}$. The eight-membered orbit is characterized by the FPV = (8, 0, 0, 0, 0, 0, 0, 0), which appears at the $(\mathbf{C}_1\backslash)\mathbf{D}_{2d}$-row of table 1. On the other hand, the set of the eight transformulas shown in the mandala (**29**) is regarded as constructing a one-membered orbit $\mathcal{G} = \{\mathcal{G}_1\}$, where we place $\mathcal{G}_1 = \{f_1, f_2, f_3, f_4, f_5, f_6, f_7, f_8\}$. Then, the one-membered orbit $\mathcal{G}$ is governed by the LCR $\mathbf{D}_{2d}(/\mathbf{D}_{2d})$. The mandala (**29**) composed of the one-membered orbit ($\mathcal{G}$) represents a molecule of $\mathbf{D}_{2d}$-symmetry. The one-membered

orbit ($\mathcal{G}$) is characterized by the FPV = (1, 1, 1, 1, 1, 1, 1, 1), which appears at the $\mathbf{D}_{2d}(/\mathbf{D}_{2d})$-row of table 1. □

4.2. *Effect of segmentation on mandalas*

4.2.1. *Mandala composed of segmented regular bodies*

Such a process of segmentation as described in example 12 is illustrated by using a mandala, as shown in figure 11.

Example 15. The process shown in example 12 is illustrated by superposing the segmentation pattern (**2**) on each of the regular bodies of the mandala shown in figure 10. The resulting diagram (figure 11) is a mandala-type illustration of figure 8. As described in example 12, this process generating a segmented regular

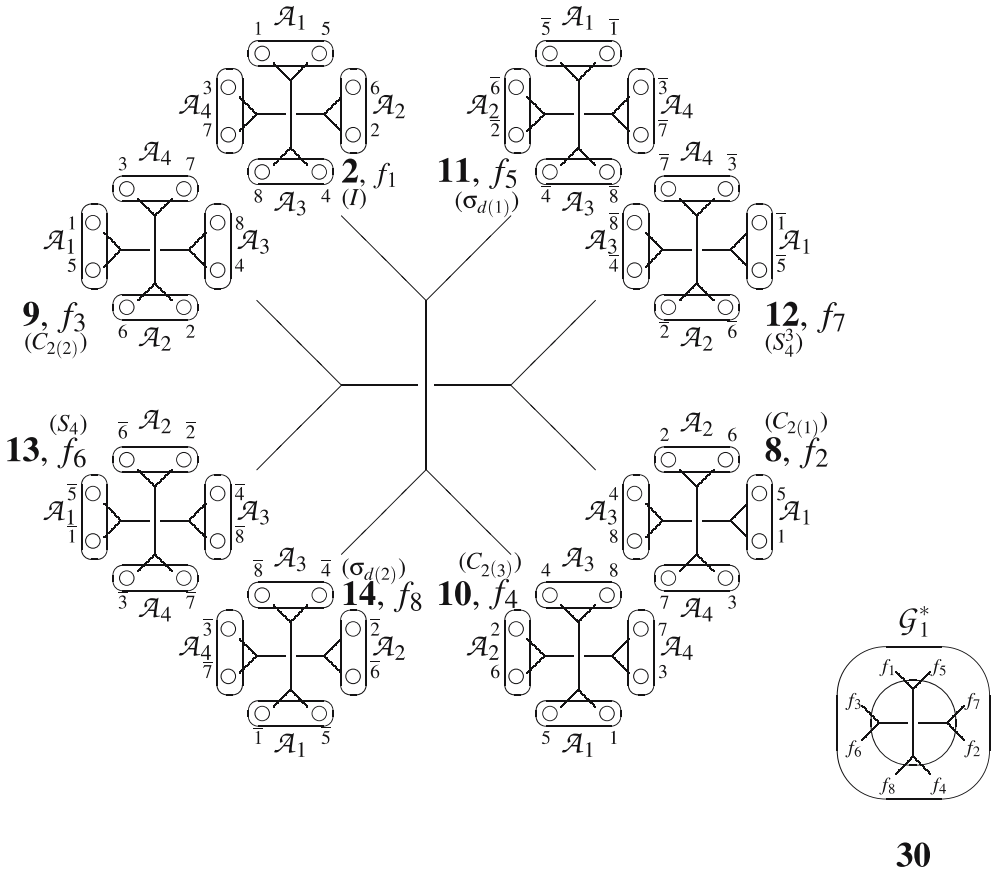

Figure 11. Mandala composed of $\mathbf{C}_s$-segmented regular bodies. The orbit of segments, $\mathcal{A} = \{\mathcal{A}_1, \mathcal{A}_2, \mathcal{A}_3, \mathcal{A}_4\}$, is characterized by an FPV = (4, 0, 0, 0, 2, 0, 0, 0, 0) so that it is governed by the RCR $(\mathbf{C}_s\backslash)\mathbf{D}_{2d}$. The full expression of the mandala is simplified into **30**.

body (**2**) maintains the $\mathbf{D}_{2d}$-symmetry of the regular body (**1**). In other words, the transformulas of the set $\mathcal{G}_1^* = \{f_1, f_2, f_3, f_4, f_5, f_6, f_7, f_8\}$ are identical if the numbering is not taken into consideration. Hence, the one-membered set $\mathcal{G}^* = \{\mathcal{G}_1^*\}$ is an orbit (equivalence class) governed by LCR $\mathbf{D}_{2d}(/\mathbf{D}_{2d})$, which is characterized by the FPV = (1, 1, 1, 1, 1, 1, 1, 1) appearing at the $\mathbf{D}_{2d}(/\mathbf{D}_{2d})$-row of table 1.

The feature of the mandala is illustrated by the simplified mandala (**30**), where the transformulas are encircled into a bundle. The mandala (**30**) composed of the one-membered orbit ($\mathcal{G}^*$) represents a molecule of $\mathbf{D}_{2d}$-symmetry.

On the other hand, the set of segments $\{\mathcal{A}_1, \mathcal{A}_2, \mathcal{A}_3, \mathcal{A}_4\}$ in each $\mathbf{C}_s$-segmented regular body is regarded as a four-membered orbit governed by the RCR $(\mathbf{C}_s\backslash)\mathbf{D}_{2d}$. The orbit is characterized by an FPV = (4, 0, 0, 0, 2, 0, 0, 0, 0), which appears at the $(\mathbf{C}_s\backslash)\mathbf{D}_{2d}$-row of table 1.

The global symmetry $\mathbf{D}_{2d}$ of the RCR $(\mathbf{C}_s\backslash)\underline{\mathbf{D}_{2d}}$ for each regular body (e.g., **2**) corresponds to the local symmetry $\mathbf{D}_{2d}$ of the LCR $\mathbf{D}_{2d}(/\underline{\mathbf{D}_{2d}})$ for the mandala (**30**). □

Obviously, the segmentation described in example 15 holds true in general cases. This is summarized as the following theorem.

Theorem 2. An **H**-segmentation in each regular body contained in a mandala of **G**-symmetry maintains the **G**-symmetry of the mandala, even if the **H** is any subgroup of the **G**.

The **H**-segmentation described in theorem 2 divides the |**G**| positions of each regular body into |**G**|/|**H**| segments, which are equivalent under **G**-symmetry. The resulting regular body with the |**G**|/|**H**| segments is called *an* **H**-*segmented regular body*, as described above. Such a segmented regular body corresponds to a molecule of **G**-symmetry, as exemplified for the $\mathbf{D}_{2d}$-symmetry in figure 6. The following theorem is derived by the preceding discussions:

Theorem 3. The set of the |**G**|/|**H**| segments in an **H**-segmented regular body is governed by the RCR (**H**\)**G**.

The mandala generated from the **H**-segmented regular body (theorem 3) consists of a one-membered **G**(/**G**)-orbit, the member of which is the set of permuted **H**-segmented regular bodies (e.g., $\mathcal{G}^* = \{\mathcal{G}_1^*\}$ of **30**). The global symmetry of the RCR (**H**\)$\underline{\mathbf{G}}$ of theorem 3 corresponds to the local symmetry of the LCR **G**(/$\underline{\mathbf{G}}$).

4.2.2. Reduced mandalas

The **H**-segments described in theorems 2 and 3 can be conceptually replaced by substitution positions (or further by proligands or atoms) to give

a reduced regular body as a secondary skeleton without the restriction of the global symmetry **G**. This type of transformation has been discussed by using figure 6 for $\mathbf{C}_s$-segments of a $\mathbf{D}_{2d}$-regular body. Thereby, the **G**-mandala with **H**-segmentation is converted into a modified one called a reduced mandala, the vertices of which accommodate reduced regular bodies such as **4**. The following example illustrates the conversion of $\mathbf{C}_s$-segments of a $\mathbf{D}_{2d}$-regular body into substitution positions so as to give a reduced mandala with reduced regular bodies as secondary skeletons.

Example 16. According to figure 6, the segmented regular body **2**, etc., in the mandala (figure 11) are replaced by the reduced regular body **4**, etc. Thereby, the corresponding reduced mandala is generated, as shown in figure 12.

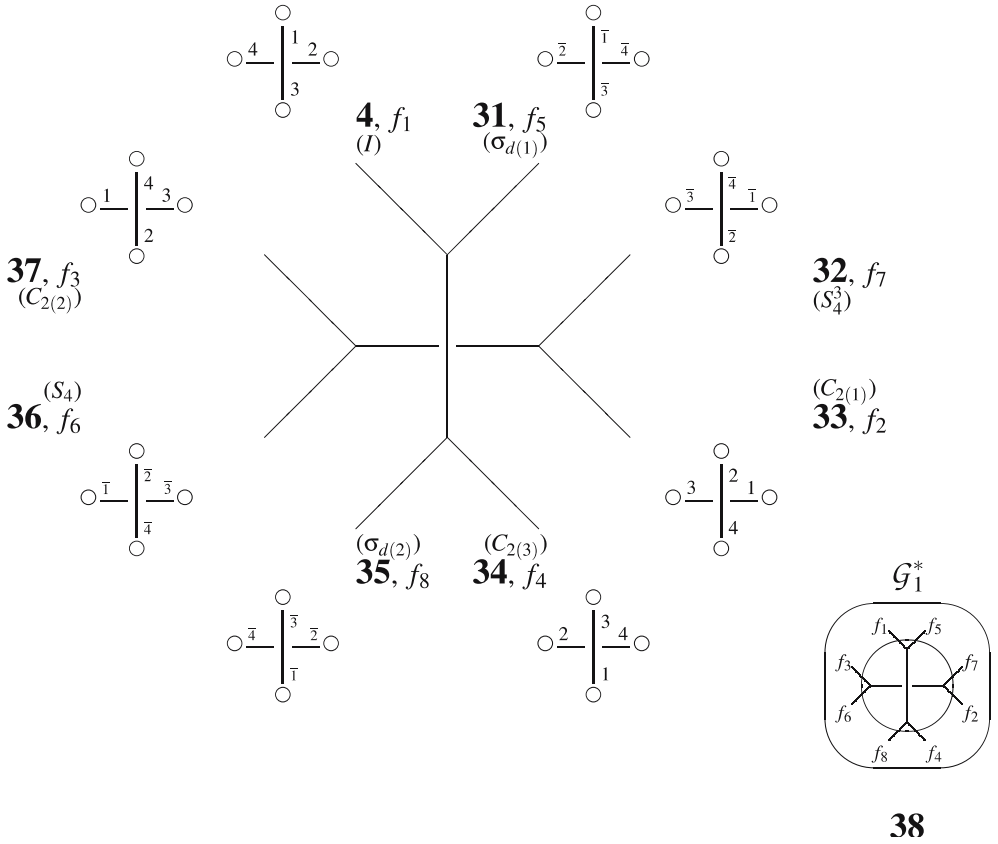

Figure 12. Reduced mandala containing eight transformulas (f_1–f_8) at its vertices. The substitution positions ($\{1, 2, 3, 4\}$) in each secondary skeleton constructs a four-membered orbit governed by the RCR $(\mathbf{C}_s\backslash)\mathbf{D}_{2d}$, which is characterized by an FPV = (4, 0, 0, 0, 2, 0, 0, 0, 0). The full expression of the mandala is simplified into **38**.

The transformulas (f_1 to f_8) generated from the reduced regular body (**4**) as a secondary skeleton are identical if the numbering is ignored so that they are encircled to give the set represented by $\mathcal{G}_1^* = \{f_1, f_2, f_3, f_4, f_5, f_6, f_7, f_8\}$ as shown in **38**. Thereby, the one-membered set ($\mathcal{G}^* = \{\mathcal{G}_1^*\}$) is an orbit (equivalence class) governed by the LCR $\mathbf{D}_{2d}(/\mathbf{D}_{2d})$. The LCR $\mathbf{D}_{2d}(/\mathbf{D}_{2d})$ is characterized by the FPV = (1, 1, 1, 1, 1, 1, 1, 1) appearing at the $\mathbf{D}_{2d}(/\mathbf{D}_{2d})$-row of table 1. As a result, the reduced mandala (**38**) composed of the one-membered orbit ($\mathcal{G}^*$) represents a molecule of $\mathbf{D}_{2d}$-symmetry, which is generated from the reduced regular body (**4**) as a secondary skeleton.

On the other hand, the set of four positions in each reduced regular body (e.g., **4** or f_1) of the reduced mandala is regarded as a four-membered orbit governed by the RCR $(\mathbf{C}_s\backslash)\mathbf{D}_{2d}$. The orbit is characterized by an FPV = (4, 0, 0, 0, 2, 0, 0, 0, 0), which appears at the $(\mathbf{C}_s\backslash)\mathbf{D}_{2d}$-row of table 1.

The global symmetry $\mathbf{D}_{2d}$ of the RCR $(\mathbf{C}_s\backslash)\underline{\mathbf{D}_{2d}}$ corresponds to the local symmetry $\mathbf{D}_{2d}$ of the LCR $\mathbf{D}_{2d}(/\underline{\mathbf{D}_{2d}})$. □

4.3. *Effect of subduction on mandalas*

4.3.1. *Assemblage of mandalas*

The diagrammatical parallelism between a regular body (e.g., **1**) and the corresponding mandala (e.g., **29**) allows us to develop a theoretical framework similar to the one described for a regular body. Thus, the concept of *segmentation* is extended to the concept of *assemblage*, by which |**G**| regular bodies placed on the vertices of a mandala of **G** are partitioned into |**G**|/|**K**| sets if the regular bodies modified are collected in agreement with a LCR (**G**(/**K**)). Such a set of equivalent transformulas is called *an assembly*.

Example 17. The feature described in figure 9 (example 13) can be illustrated by starting from the $\mathbf{D}_{2d}$-mandala depicted in figure 10. By superposing the subduction pattern (**6**) on each regular body contained in figure 10, we obtain figure 13, which shows the $\mathbf{C}_s$-assemblage of the $\mathbf{D}_{2d}$-mandala. Obviously, this figure has the same meaning as figure 9. The resulting assemblies, i.e., $\mathcal{A}_1^* = \{f_1, f_5\}, \mathcal{A}_2^* = \{f_2, f_7\}, \mathcal{A}_3^* = \{f_4, f_8\}$, and $\mathcal{A}_4^* = \{f_3, f_6\}$, are shown in the simplified mandala (**47**). These assemblies construct a four-membered orbit of assemblies, i.e., $\mathcal{A} = \{\mathcal{A}_1^*, \mathcal{A}_2^*, \mathcal{A}_3^*, \mathcal{A}_4^*\}$, which is governed by the LCR $\mathbf{D}_{2d}(/\mathbf{C}_s)$, as discussed later in detail.

The procedure of constructing figure 13 can be interpreted inversely. We first consider the $\mathbf{C}_s$-assemblage, where one of the $\mathbf{C}_s$-assemblies (e.g., $\mathcal{A}_1^* = \{f_1, f_5\}$) is selected. This selection is inevitably accompanied by the $\mathbf{C}_s$-subduction. Thus, the $\mathbf{C}_s$-assembly $\{f_1, f_5\}$ (={**6**, **18**}) means the restriction of the $\mathbf{D}_{2d}$-regular body into $\mathbf{C}_s$. The restriction results in the subduction $(\mathbf{C}_1\backslash)\mathbf{D}_{2d} \downarrow \mathbf{C}_s$ with respect to the eight positions of the regular body, as shown in equation

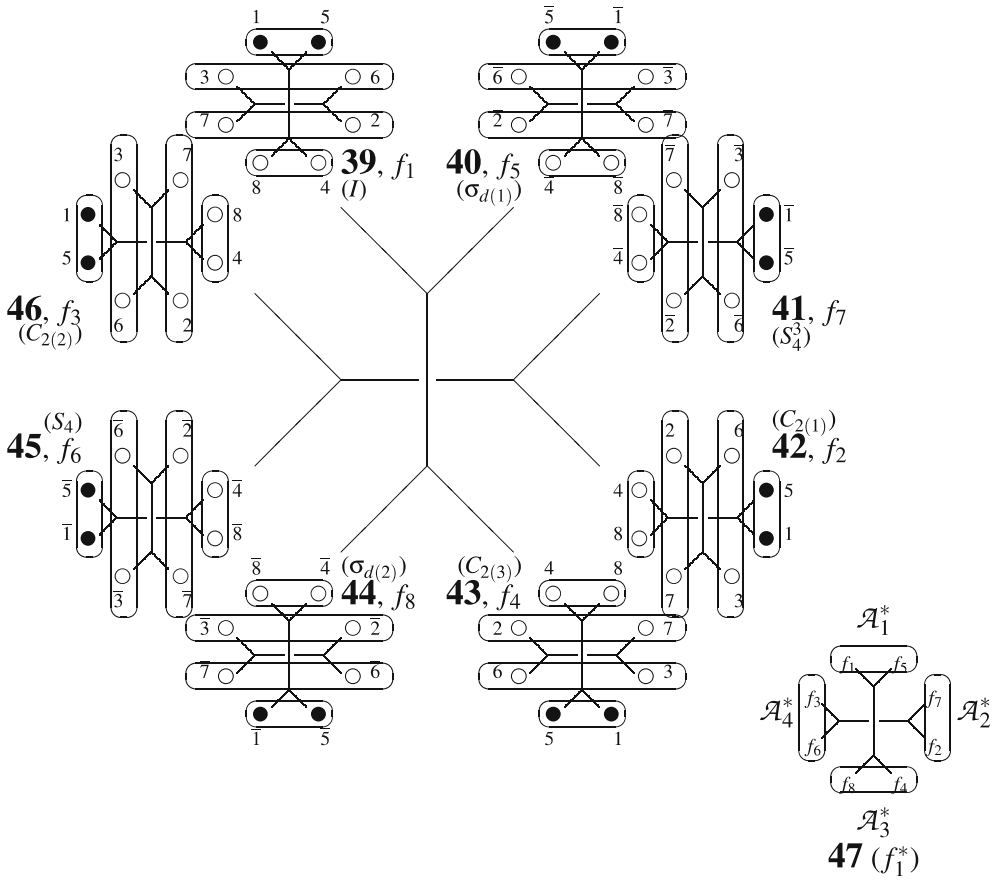

Figure 13. Mandala (a nested regular body) after $\mathbf{C}_s$-assemblage. The eight transformulas (f_1–f_8) at its vertices are assembled into four assemblies, i.e., $\mathcal{A}_1^* = \{f_1, f_5\}$, $\mathcal{A}_2^* = \{f_2, f_7\}$, $\mathcal{A}_3^* = \{f_4, f_8\}$, and $\mathcal{A}_4^* = \{f_3, f_6\}$. The alignment shown in this diagram, in which solid circles are added to show the $\mathbf{C}_s$-symmetry explicitly, corresponds to the right diagram shown in figure 9. The full expression of the mandala is simplified into **47**.

(80) of example 11. Thereby, the eight positions are partitioned, as shown in **6** (figure 9) or in each of the regular bodies appearing in figure 13. This partition produces a diagram of a more chemical meaning, e.g., **7**, as shown in figure 7. Note that the global symmetry $\mathbf{C}_s$ of the four RRRs $(\mathbf{C}_1\backslash)\underline{\mathbf{C}_s}$ corresponds to the local symmetry of the LCR $\mathbf{D}_{2d}(/\underline{\mathbf{C}_s})$ of the assembled mandala (**47**). □

The discussions in example 17 can be easily generalized so as to give the following theorem:

Theorem 4. A **K**-assembly in a mandala of **G**-symmetry contains |**K**| regular bodies of **K**-symmetry. The |**G**| positions of each regular body suffers from **K**-subduction so as to cause the subduction $(\mathbf{C}_1\backslash)\mathbf{G} \downarrow \mathbf{K}$.

The **K**-assemblage described in theorem 4 generates |**G**|/|**K**| assemblies equivalent under **G**-symmetry. The resulting mandala with the |**G**|/|**K**| assemblies is called *a* **K**-*assembled mandala*. The following theorem is derived by the preceding discussions:

Theorem 5. The set of |**G**|/|**K**| assemblies in a **K**-assembled mandala is governed by the LCR **G**(/**K**).

It is to be noted that the mode of assemblage in the mandala **47**, i.e., $\{f_1, f_5\}, \{f_2, f_7\}, \{f_4, f_8\}$, and $\{f_3, f_6\}$, corresponds to the mode of subduction in the regular body **39**, i.e., {1, 5}, {2, 7}, {4, 8}, and {3, 6}. This correspondence is assured by selecting the reference numbering for the regular body and the inverse numbering for the mandala (cf. figure 4).

4.3.2. Nested mandalas

In order to assure the equivalence of the |**G**|/|**K**| assemblies under **G** (theorem 5), the **K**-assembled mandala (e.g., **47**) should be permuted by the operations of **G**. This means the consideration of *a nested mandala* defined as follows:

Definition 2. Suppose that a mandala f_1^* is given, where the |**G**|-membered set of regular bodies in the mandala is governed by the LRR $\mathbf{G}(/\mathbf{C}_1)$ (cf. equation (74)). Then, permuted mandalas f_1^*–$f_{|\mathbf{G}|}^*$, which are generated from the mandala (f_1^*) by the permutations due to the group **G**, are placed on the vertices of a hypothetical regular body in accord with the RRR $(\mathbf{C}_1\backslash)\mathbf{G}$ (cf. equation (65)) corresponding to the LRR. The resulting diagram is called *a nested mandala* of the group **G**.

Each mandala contained in such a nested mandala may be assembled to give a |**G**|/|**K**|-membered set of assemblies. Whether such assemblage is involved or not, |**G**| of the mandalas construct a one-membered orbit governed by the RRR $(\mathbf{G}\backslash)\mathbf{G}$. Thereby, the |**G**|/|**K**|-membered set of the assemblies is governed by the LCR **G**(/**K**). Theorem 2 for characterizing a mandala is rewritten for the present case of a nested mandala as follows:

Theorem 6. A **K**-assemblage of each mandala contained in a nested mandala of **G**-symmetry maintains the **G**-symmetry of the nested mandala, where the **K** is any subgroup of the **G**.

According to theorem 6, the **K**-assemblage represents a molecule of **K**-symmetry. The following example illustrates a nested mandala for the $\mathbf{D}_{2d}$-symmetry.

Example 18. The assembled mandala (**47**) is adopted a reference mandala (f_1^*). They are permuted by means of $\mathbf{D}_{2d}$ so as to generate a nested mandala shown in figure 14. Each of the generated mandalas (f_1^*–f_8^*), where an overbar is used to designate the alternation of chirality in each of the regular bodies (f_1–f_8). The set of mandalas in the nested mandala (figure 14), i.e., $\mathcal{G}_1^\dagger = \{f_1^*, f_2^*, f_3^*, f_4^*, f_5^*, f_6^*, f_7^*, f_8^*\}$, is superposed onto itself under $\mathbf{D}_{2d}$. In other words, the corresponding one-membered set $\mathcal{G}^\dagger = \{\mathcal{G}_1^\dagger\}$ is an equivalence class (orbit) governed by the RCR $(\mathbf{D}_{2d}\backslash)\mathbf{D}_{2d}$, as shown in the corresponding simplified nested mandala (**55**).

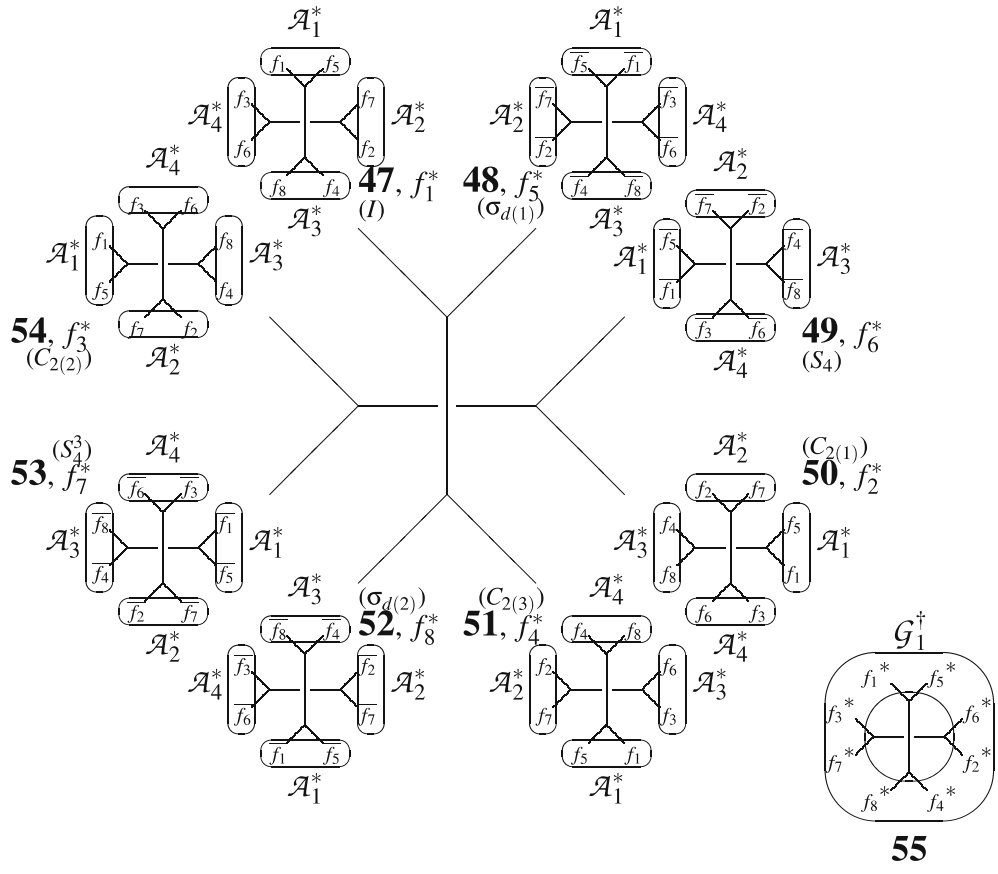

Figure 14. Nested mandala. This figure is characterized by an FPV = (4, 0, 0, 0, 2, 0, 0, 0, 0) with respect to the orbit of assemblies, $\mathcal{A}^* = \{\mathcal{A}_1^*, \mathcal{A}_2^*, \mathcal{A}_3^*, \mathcal{A}_4^*\}$, which is governed by the LCR $\mathbf{D}_{2d}(/\mathbf{C}_s)$. The full expression of the mandala is simplified into **55**.

According to theorem 6, the $\mathbf{C}_s$-assemblage of each mandala in the nested mandala shown in figure 14 maintains the $\mathbf{D}_{2d}$-symmetry of the nested mandala. As a result, the four sets of assemblies in each mandala, i.e., $\mathcal{A}_1^* = \{f_1, f_5\}$, $\mathcal{A}_2^* = \{f_2, f_7\}$, $\mathcal{A}_3^* = \{f_4, f_8\}$, and $\mathcal{A}_4^* = \{f_3, f_6\}$, construct a four-membered equivalence class (orbit) governed by the LCR $\mathbf{D}_{2d}(/\mathbf{C}_s)$. The global symmetry of the LCR $\mathbf{D}_{2d}(/\mathbf{C}_s)$ for the mandalas (e.g., **47**, f_1^*) corresponds to the local symmetry of the RCR $(\underline{\mathbf{D}_{2d}}\backslash)\mathbf{D}_{2d}$ for the nested mandala (**55**). □

4.4. Characterization of symmetry equivalency

4.4.1. Parallelism between mandalas and nested mandalas

The comparison between definition 1 for a mandala (i.e., a nested regular body) and definition 2 for a nested mandala shows a mathematical parallelism between the two relationships, i.e., (1) the relationship between a regular body and a mandala (a nested regular body) and (2) the relationship between a mandala and a nested mandala.

The relationship between a regular body and a mandala (a nested regular body) is shown in figure 15, where the maintenance of the $\mathbf{D}_{2d}$-symmetry is found in various types of mandalas, e.g., the mandala (**29**) derived from the regular body (**1**), the mandala (**30**) derived from the segmented regular body (**2**), and the mandala (**38**) derived from the reduced regular body (**4**). It should be emphasized that the diagrams for these types of mandalas are identical with each other in the level of simplified expressions, as shown in figure 15. If the types of mandalas should be specified, a mandala with segmented regular bodies (e.g., **30**) is called *a segmented mandala* and a mandala with reduced regular bodies (e.g., **38**) is called *a reduced mandala*.

The maintenance of the $\mathbf{D}_{2d}$-symmetry means the common global symmetry $\mathbf{D}_{2d}$ for the eight-membered $(\mathbf{C}_1\backslash)\mathbf{D}_{2d}$-orbit of $\mathbf{C}_1$-segments in the regular body (**1**), the four-membered $(\mathbf{C}_s\backslash)\mathbf{D}_{2d}$-orbit of $\mathbf{C}_s$-segments in the segmented regular body (**2**), and the four-membered $(\mathbf{C}_s\backslash)\mathbf{D}_{2d}$-orbit of $\mathbf{C}_s$-positions (or proligands) in the reduced regular body (**4**). As a result, such tables as shown in tables 1, 2, and 4 are effective commonly to these cases. It should be noted that a one-membered $(\mathbf{D}_{2d}\backslash)\mathbf{D}_{2d}$-orbit of a $\mathbf{D}_{2d}$-segment is possible as an alternative extreme case.

On the other hand, the relationship between a mandala and a nested mandala is shown in figure 16, where the mandalas with no assemblies (**29**, **30**, and **38**) are first taken into consideration and the assembled mandala (**47**) are next considered. Both of them are linked to the nested mandala (**55**), which shows the maintenance of the $\mathbf{D}_{2d}$-symmetry of the nested mandala.

The maintenance of the $\mathbf{D}_{2d}$-symmetry means the common global symmetry $\mathbf{D}_{2d}$ for the one-membered $\mathbf{D}_{2d}(/\mathbf{D}_{2d})$-orbit $(\mathcal{G})$ of the $\mathbf{D}_{2d}$-assembly $(\mathcal{G}_1^*)$ in each of the non-assembled mandalas (**29**, **30**, and **38**) and the four-membered

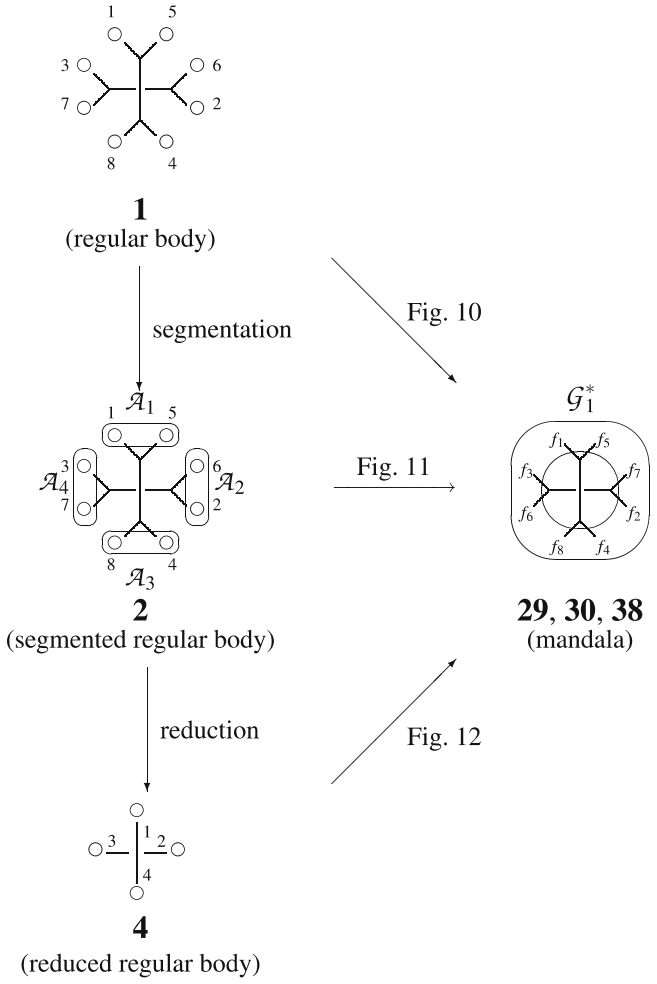

Figure 15. Mandala related to a regular body, a segmented regular body, and a reduced regular body. When the types of mandalas should be specified, a mandala with segmented regular bodies (e.g., **30**) is called *a segmented mandala* and a mandala with reduced regular bodies (e.g., **38**) is called *a reduced mandala*.

$\mathbf{D}_{2d}(/\mathbf{C}_s)$-orbit ($\mathcal{A} = \{\mathcal{A}_1^*, \mathcal{A}_2^*, \mathcal{A}_3^*, \mathcal{A}_4^*\}$) of $\mathbf{C}_s$-assemblies in the assembled mandala (**47**). Anyone of the assemblies (e.g., $\mathcal{A}_1^*$) represents a molecule of $\mathbf{C}_s$-symmetry. As a result, such tables as shown in tables 1, 2, and 4 are also effective commonly to these cases. It should be noted that an eight-membered $\mathbf{D}_{2d}(/\mathbf{C}_1)$-orbit of a $\mathbf{C}_1$-assembly is possible as an alternative extreme case.

On the same line as the reduction process shown in figure 15, we are able to consider an equivalent process called *coalescence*, i.e., the process of the assembled mandalas into **56**, in which f_1 and f_5 coalesce into g_1 and so on. The

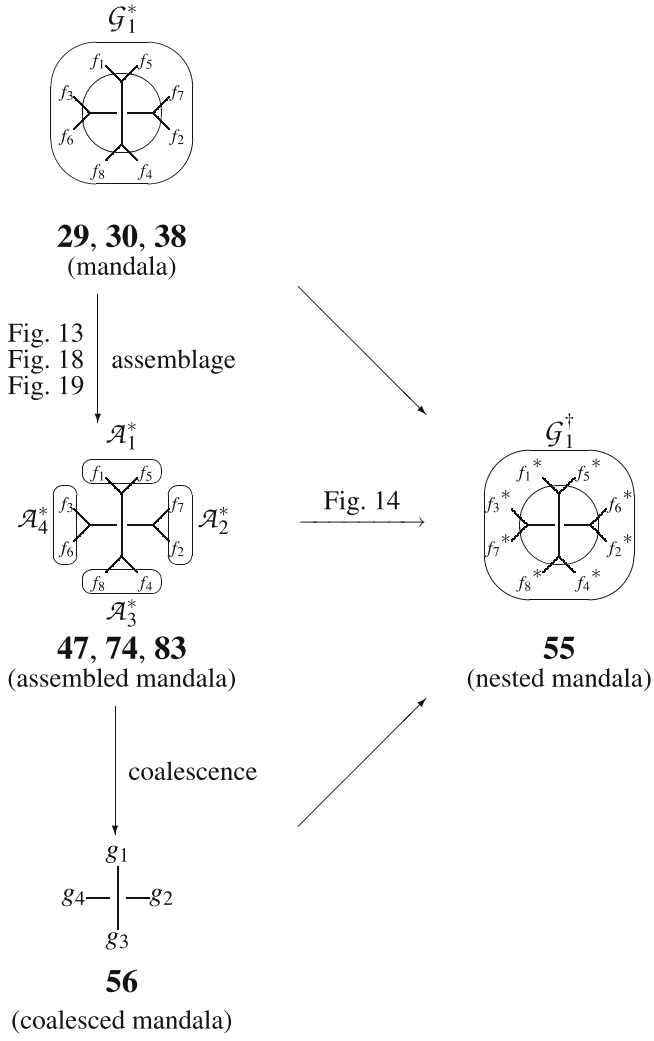

Figure 16. Nested mandala related to a mandala, an assembled mandala, and a coalesced mandala.

coalescence process indicates a molecule of $\mathbf{C}_s$-symmetry to be counted once in stereoisomer enumeration.

4.4.2. Fixed segments and fixed assemblies

As can be seen easily by their definitions, regular bodies of **G**-symmetry and mandalas of **G**-symmetry have diagrammatically equivalent features from a mathematical point of view. In particular, the comparison between segmented regular bodies (cf. figure 15 for the $\mathbf{D}_{2d}$-symmetry) and assembled mandalas (cf. figure 16 for the $\mathbf{D}_{2d}$-symmetry) reveals these equivalent features. The features are more clearly demonstrated by regarding both the positions of a reg-

ular body and the regular bodies of a mandala as "abstract" points which are governed by an RRR or an LRR. Thereby, the segmentation of a regular body and the assemblage of a mandala can be regarded as representing a mathematically equivalent procedure. Thus, a set of **H**-segments (cf. **2**) in a regular body of **G**-symmetry is determined to be an orbit governed by an RCR (**H**\)**G** by means of a mandala (cf. **47**). On the same line, a set of **K**-assemblies (cf. **47**) in a mandala of **G**-symmetry is determined to be an orbit governed by a LCR **G**(/**K**) by means of a nested mandala (**55**). This means that the set of segments governed by an RCR (**H**\)**G** (cf. **2**) and the set of assemblies governed by a LCR **G**(/**K**) (cf. **47**) are both characterized by FPVs described in section 2.2. If **K** = **H**, a common FPV can be used because the RCR (**H**\)**G** and the LCR **G**(/**H**) are regarded as equivalent, as described in theorem 1. Note that the symmetry of the mandala determines the global symmetry **G** and the symmetry of each segment determines the local symmetry **H** and that the symmetry of the nested mandala determines the global symmetry **G** and the symmetry of each assembly determines the local symmetry **K**.

Example 19. The orbit $\mathcal{A} = \{\mathcal{A}_1, \mathcal{A}_2, \mathcal{A}_3, \mathcal{A}_4\}$ shown in figure 11 is examined by taking account of the SSG of $\mathbf{D}_{2d}$ (equation (19)). Thereby, the number of fixed segments with respect to each subgroup of the SSG is obtained. For example, by the restriction of the $\mathbf{D}_{2d}$-symmetry into $\mathbf{C}_s$-symmetry, the two segments $\mathcal{A}_1$ and $\mathcal{A}_3$ are fixed but $\mathcal{A}_2$ and $\mathcal{A}_4$ are interchanged. It follows that the mark of this case is determined to be 2. This is the fifth number of the corresponding FPV = (4, 0, 0, 0, 2, 0, 0, 0, 0), which is obtained by repeating this procedure to cover the SSG of $\mathbf{D}_{2d}$ (equation (19)). Because the FPV is found at the ($\mathbf{C}_s$\)$\mathbf{D}_{2d}$-row of table 1, it shows that the four-membered orbit $\mathcal{A}$ is governed by the RCR ($\mathbf{C}_s$\)$\mathbf{D}_{2d}$. It should be noted that the orbit $\mathcal{A}$ is concerned with the substitution positions of the regular body at issue.

On the other hand, the orbit $\mathcal{A}^* = \{\mathcal{A}_1^*, \mathcal{A}_2^*, \mathcal{A}_3^*, \mathcal{A}_4^*\}$ shown in figure 14 is examined by taking account of the SSG of $\mathbf{D}_{2d}$ (equation (19)). Thereby, the number of fixed assemblies with respect to each subgroup of the SSG is obtained so as to give an FPV = (4, 0, 0, 0, 2, 0, 0, 0, 0). For example, the $\mathbf{C}_s$-restriction fixes two assemblies (i.e., $\mathcal{A}_1^*$ and $\mathcal{A}_3^*$) so as to give a mark (2), which is the fifth number of the FPV. Because the FPV is found at the $\mathbf{D}_{2d}$(/$\mathbf{C}_s$)-row of table 1, the four-membered obit $\mathcal{A}^*$ is concluded to be governed by the LCR $\mathbf{D}_{2d}$(/$\mathbf{C}_s$). It should be noted that the orbit $\mathcal{A}^*$ is concerned with the transformulas of the mandala at issue. □

4.5. Subduction linking segmentation and assemblage

In the preceding discussions, segmentation in a regular body and assemblage in a mandala are treated rather separately. In the present subsection, we

shall show that the superposition of segmentation and subduction causes assemblage in a mandala and that the consideration of assemblage in a mandala results in the subduction of segmented regular bodies.

4.5.1. Superposition of segmentation and subduction

The effect of segmentation and that of subduction can be superposed to generate a further modified mandala. The following example illustrates the superposition of the segmentation shown in figure 11 onto the subduction shown in figure 13.

Example 20. The mandala generated by the segmentation shown in figure 11 is superposed onto the mandala generated by the subduction (figure 13), where the subduction pattern is omitted for the sake of simplicity. Thereby, we obtain another mandala shown in figure 17, where the same mode of assemblage as shown in figure 13 takes place to generate **65**, which contains a set of four $\mathbf{C}_s$-assemblies, i.e., $\mathcal{A}^* = \{\mathcal{A}_1^*, \mathcal{A}_2^*, \mathcal{A}_3^*, \mathcal{A}_4^*\}$.

The set of four $\mathbf{C}_s$-assemblies $\mathcal{A}^*$ in **65** (f_1^*) is a four-membered orbit governed by the LCR $\mathbf{D}_{2d}(/\mathbf{C}_s)$, where the LCR is characterized by an FPV = (4, 0, 0, 0, 2, 0, 0, 0, 0). This result is confirmed by the fact that **65** (f_1^*) exhibits the same behavior as illustrated in the nested mandala shown in figure 14.

On the other hand, the set of four $\mathbf{C}_s$-segments in each transformula (e.g., **57**), i.e., $\mathcal{A} = \{\mathcal{A}_1, \mathcal{A}_2, \mathcal{A}_3, \mathcal{A}_4\}$, suffers from the subduction $(\mathbf{C}_s\backslash)\mathbf{D}_{2d} \downarrow \mathbf{C}_s$, which is associated with the $\mathbf{C}_s$-assemblage. In agreement with equation (63), the orbit $\mathcal{A}$ is divided into a one-membered suborbit $\{\mathcal{A}_1\}$, a two-membered suborbit $\{\mathcal{A}_2, \mathcal{A}_4\}$, and another one-membered suborbit $\{\mathcal{A}_3\}$. Chemically speaking, if the segment $\{\mathcal{A}_1\}$ is substituted by a proligand A, each of $\{\mathcal{A}_2, \mathcal{A}_4\}$ by a proligand B, and $\{\mathcal{A}_3\}$ by a proligand X, there emerges an allene derivative with AB_2X, which belongs to $\mathbf{C}_s$-symmetry. □

The following example illustrates the inversely ordered superposition of the subduction shown in figure 13 onto the segmentation shown in figure 11.

Example 21. The $\mathbf{D}_{2d}$-symmetry of the mandala generated by the segmentation shown in figure 11 is restricted into $\mathbf{C}_s$, as shown in figure 18. This process is equivalent to the superposition of the mandala generated by the subduction (figure 13), although the illustrated form is slightly different. Thereby, we obtain another mandala shown in figure 18, where the same mode of assemblage as shown in figure 13 takes place to generate **74**. The resulting set of four $\mathbf{C}_s$-assemblies, i.e., $\mathcal{A}^* = \{\mathcal{A}_1^*, \mathcal{A}_2^*, \mathcal{A}_3^*, \mathcal{A}_4^*\}$ is governed by the LCR $\mathbf{D}_{2d}(/\mathbf{C}_s)$, which is characterized by an FPV = (4, 0, 0, 0, 2, 0, 0, 0, 0).

On the same line as illustrated by example 20, the set of four $\mathbf{C}_s$-segments in each transformula (e.g., **66**) suffers from the subduction $(\mathbf{C}_s\backslash)\mathbf{D}_{2d} \downarrow \mathbf{C}_s$, which is associated with the $\mathbf{C}_s$-assemblage. Thereby, the orbit $\mathcal{A} = \{\mathcal{A}_1, \mathcal{A}_2, \mathcal{A}_3, \mathcal{A}_4\}$ is

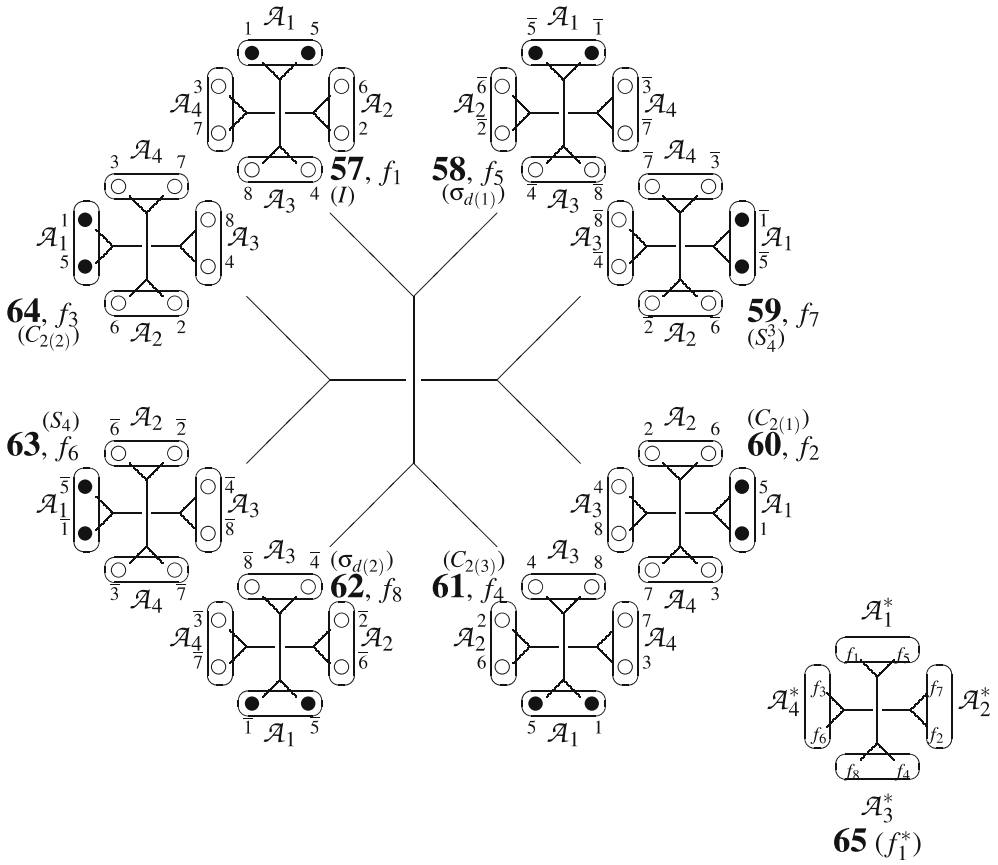

Figure 17. Mandala modified by the superposition of $\mathbf{C}_s$-segmentation and $\mathbf{C}_s$-subduction. The eight transformulas (f_1–f_8) at its vertices are assembled into four assemblies, i.e., $\mathcal{A}_1^* = \{f_1, f_5\}$, $\mathcal{A}_2^* = \{f_2, f_7\}$, $\mathcal{A}_3^* = \{f_4, f_8\}$, and $\mathcal{A}_4^* = \{f_3, f_6\}$. The alignment shown in this diagram, in which solid circles are added to show the $\mathbf{C}_s$-symmetry explicitly, corresponds to the right diagram shown in figure 9. The full expression of the mandala is simplified into **65**.

divided into two one-membered suborbits ($\{\mathcal{A}_1\}$ and $\{\mathcal{A}_3\}$) and a two-membered suborbit $\{\mathcal{A}_2, \mathcal{A}_4\}$ in agreement with equation (63). On the same line as example 20, the devision of $\mathcal{A}$ corresponds to an allene derivative with AB_2X, which belongs to $\mathbf{C}_s$-symmetry. □

Examples 20 and 21 can be discussed more chemically by the subduction of the reduced mandala shown in figure 12.

Example 22. The mandala generated by the segmentation shown in figure 11 is symmetrically equivalent to the reduced mandala shown in figure 12, where the common $\mathbf{D}_{2d}$ symmetry is confirmed by the comparison between **30** and **38**.

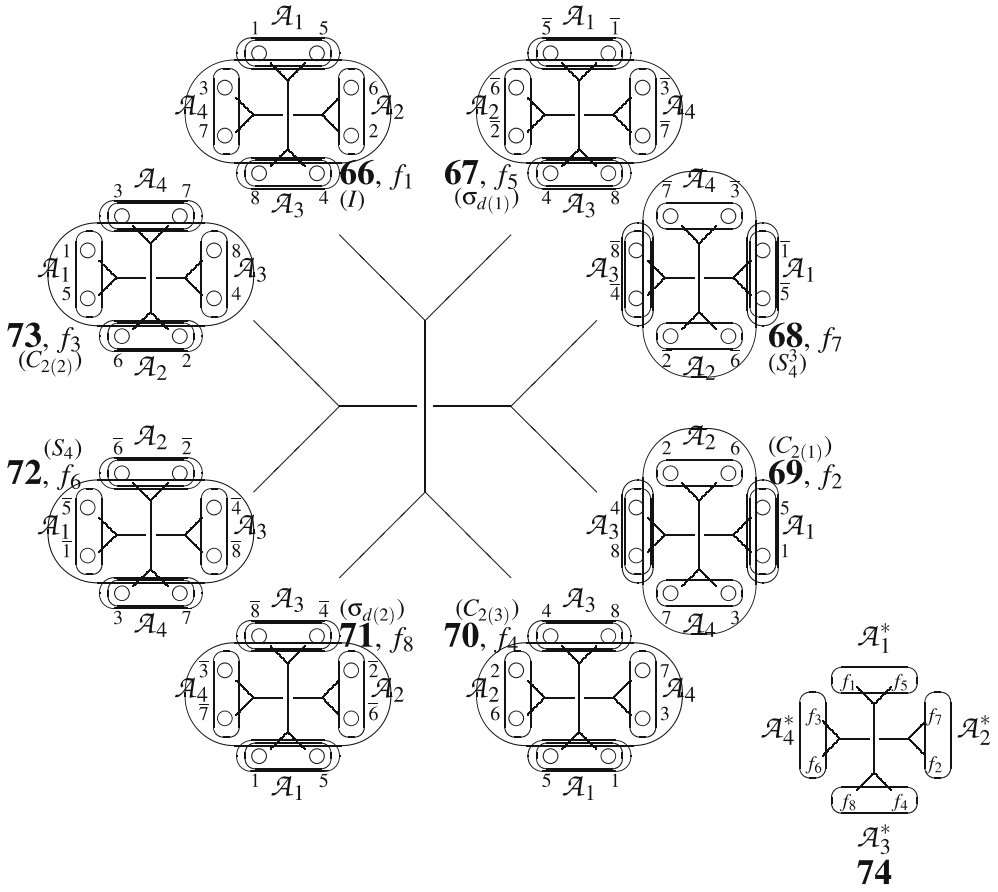

Figure 18. Subduction of a segmented mandala for representing the superposition of subduction onto segmentation. The full expression of the mandala is simplified into **74**.

The process discussed in example 21 is alternatively illustrated by the subduction of each transformula (e.g., **4**) contained in the reduced mandala shown in figure 12. Thereby, we obtain another mandala shown in figure 19, where the same mode of assemblage as shown in figures 17 or 18 takes place so as to generate **83**. The resulting set of four $\mathbf{C}_s$-assemblies, i.e., $\mathcal{A}^* = \{\mathcal{A}_1^*, \mathcal{A}_2^*, \mathcal{A}_3^*, \mathcal{A}_4^*\}$, is governed by the LCR $\mathbf{D}_{2d}(/\mathbf{C}_s)$, which is characterized by an FPV $= (4, 0, 0, 0, 2, 0, 0, 0, 0)$.

The orbit of four substitution positions $\{1, 2, 3, 4\}$ in each transformula (e.g., **75**) suffers from the subduction $(\mathbf{C}_s\backslash)\mathbf{D}_{2d} \downarrow \mathbf{C}_s$, which is associated with the $\mathbf{C}_s$-assemblage. Thereby, the orbit is divided into two one-membered suborbits ($\{1\}$ and $\{3\}$) and a two-membered suborbit $\{2, 4\}$ in agreement with equation (63). On the same line as examples 20 and 21, the devision of the orbit

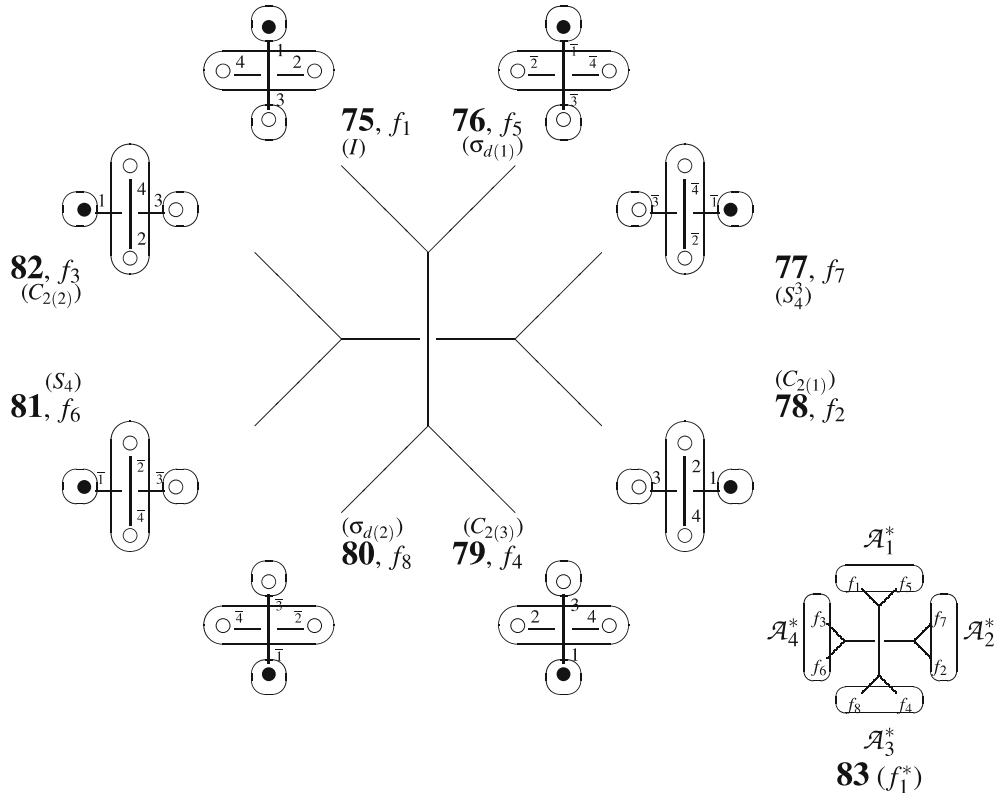

Figure 19. Reduced mandala after assemblage. The eight transformulas (f_1–f_8) are assembled into four assemblies, i.e., $\mathcal{A}_1^* = \{f_1, f_5\}, \mathcal{A}_2^* = \{f_2, f_7\}, \mathcal{A}_3^* = \{f_4, f_8\}$,and $\mathcal{A}_4^* = \{f_3, f_6\}$. The full expression of the mandala is simplified into **83**.

corresponds to an allene derivative with AB_2X, which belongs to $\mathbf{C}_s$-symmetry. □

4.5.2. Subduction due to assemblage

The subduction of a regular body shown in figure 13, the subduction of a segmented regular body shown in figures 17 and 18, and the subduction of a reduced regular body shown in figure 19 are summarized by the superposition of subduction patterns onto figure 15. Thereby, we obtain figure 20.

The non-assembled mandalas (**29**, **30**, and **38**) shown in figure 15 indicates no subduction of regular bodies (e.g., **1**), segmented regular bodies (e.g., **2**), and reduced regular bodies (e.g., **4**), where the corresponding RCRs are characterized by the global symmetry $\mathbf{D}_{2d}$.

On the other hand, the assembled mandala (**47**, **65**, **74**, and **83**) shown in figure 20 indicates the $\mathbf{C}_s$-subduction of regular bodies (e.g., **39**), segmented

regular bodies (e.g., **57** and **66**), and reduced regular bodies (e.g., **75**), where the corresponding RCRs are characterized by the global symmetry $\mathbf{C}_s$.

For the sake of convenience for further discussions, theorem 5 should be restated so as to demonstrate its chemical meaning more clearly in the following theorem:

Theorem 7. One assembled mandala of **G**-symmetry having $|\mathbf{G}|/|\mathbf{K}|$ of **K**-assemblies corresponds to one *molecule* of **K**-symmetry, where the orbit of the **K**-assemblies is governed by the LCR $\mathbf{G}(/\mathbf{K})$.

Note that the assembled mandala of **G**-symmetry described in theorem 7 may be derived by the subduction of regular bodies, segmented regular bodies, or reduced regular bodies, as exemplified in figure 20. The subduction of reduced regular bodies has a more chemical meaning than the others.

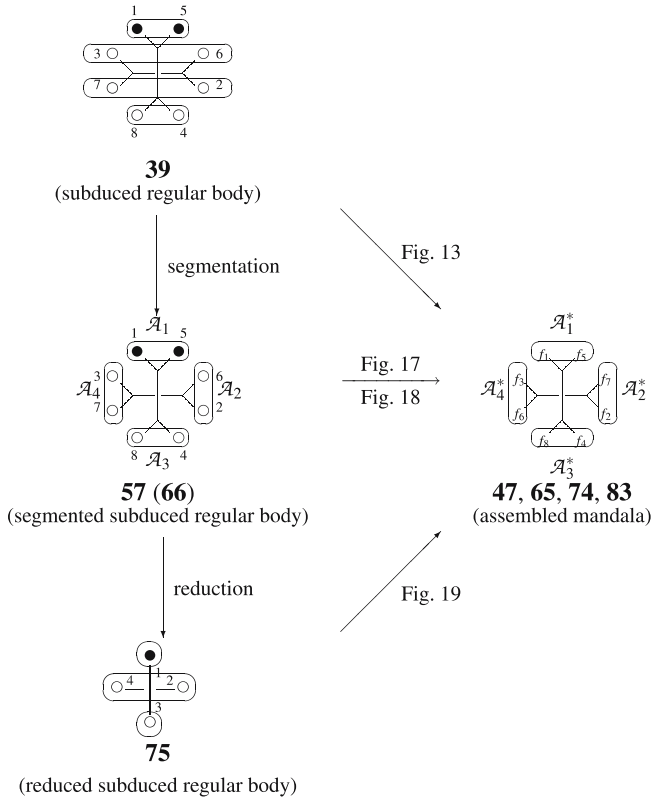

Figure 20. Assembled mandala related to a subduced regular body, a segmented subduced regular body, and a reduced subduced regular body.

5. Combinatorial enumeration

5.1. Row view for evaluating fixed-point vectors

According to theorem 7, the FPV for the LCR **G**(/**K**) is used to characterize one molecule of **K**-symmetry, which is derived from a skeleton of **G**-symmetry. For example, suppose that each solid circle is replaced by X and each open circle is replaced by H in figure 19. This procedure is regarded as a function f, which is specified as $f(1) = \mathrm{X}$, $f(2) = \mathrm{H}$, $f(3) = \mathrm{H}$, and $f(4) = \mathrm{H}$. Thereby, we obtain figure 21, where the orbit of assemblies, i.e., $\mathcal{A}^* = \{\mathcal{A}_1^*, \mathcal{A}_2^*, \mathcal{A}_3^*, \mathcal{A}_4^*\}$, is governed by the LCR $\mathbf{D}_{2d}(/\mathbf{C}_s)$, which is characterized by an FPV = (4, 0, 0, 2, 0, 0, 0, 0) (cf. table 1). The FPV gives the coefficients for the terms $4\mathrm{H}^3\mathrm{X}$ for $\mathbf{D}_{2d}$ and $2\mathrm{H}^3\mathrm{X}$ for $\mathbf{C}_s$ so that it corresponds to one allene derivative with mono-X-substitution.

Another procedure to realize the $\mathbf{C}_s$-symmetry is possible on the basis of figure 19, where another function f is specified as $f(1) = \mathrm{X}$, $f(2) = \mathrm{p}$, $f(3) = \mathrm{H}$, and $f(4) = \overline{\mathrm{p}}$. Thereby, we obtain figure 22, where the orbit of assemblies, i.e., $\mathcal{A}^* = \{\mathcal{A}_1^*, \mathcal{A}_2^*, \mathcal{A}_3^*, \mathcal{A}_4^*\}$, is governed by the LCR $\mathbf{D}_{2d}(/\mathbf{C}_s)$, which is characterized by an FPV = (4, 0, 0, 2, 0, 0, 0, 0) (cf. table 1). The FPV gives the

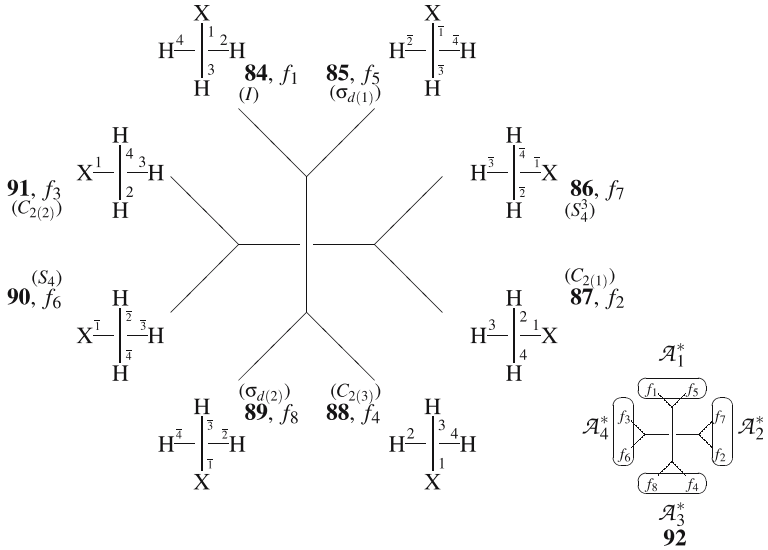

Figure 21. Reduced mandala with $\mathbf{C}_s$-transformulas derived from an allene skeleton, where a spontaneous assemblage occurs, as shown in a simplified assembly (**92**). Thus, the $\mathbf{C}_s$-transformulas are spontaneously assembled into four assemblies (**84/85**, **86/87**, **88/89**, and **90/91**), which construct a four-membered orbit governed by the CR $\mathbf{D}_{2d}(/\mathbf{C}_s)$. The orbit (representing a mono-X-allene molecule) is characterized by a fixed-point vector: (4, 0, 0, 2, 0, 0, 0, 0).

coefficients for the terms 4HXp$\overline{\text{p}}$ for $\mathbf{D}_{2d}$ and 2HXp$\overline{\text{p}}$ $\mathbf{C}_s$ so that it corresponds to one allene derivative with the molecular formula HXp$\overline{\text{p}}$.

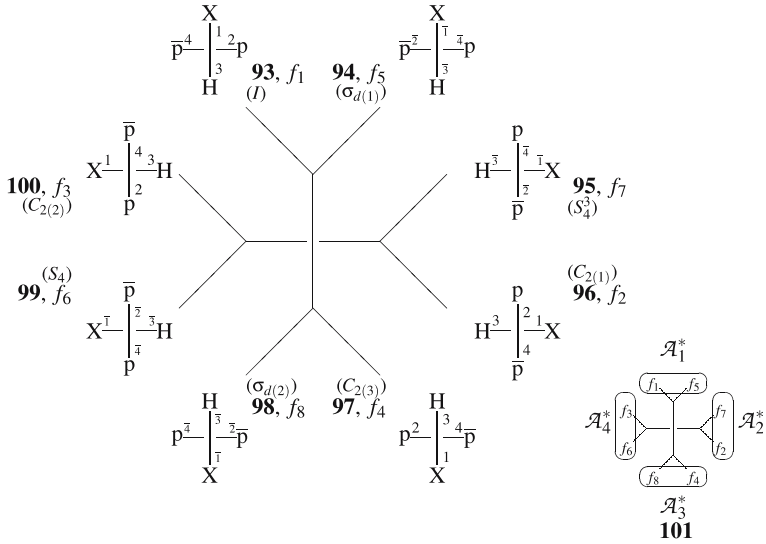

Figure 22. Reduced mandala with $\mathbf{C}_s$-transformulas derived from an allene skeleton, where a spontaneous assemblage occurs, as shown in a simplified assembly (**101**). Thus, the $\mathbf{C}_s$-transformulas are spontaneously assembled into four assemblies (**93/94**, **95/96**, **97/98**, and **99/100**), which construct a four-membered orbit governed by the CR $\mathbf{D}_{2d}(/\mathbf{C}_s)$. The orbit (representing an allene molecule with HXp$\overline{\text{p}}$) is characterized by a fixed-point vector: (4, 0, 0, 2, 0, 0, 0, 0).

It should be noted a further function f (i.e., $f(1) = \text{X}$, $f(2) = \overline{\text{p}}$, $f(3) = \text{H}$, and $f(4) = \text{p}$) generated another achiral derivative of $\mathbf{C}_s$-symmetry on the basis of figure 19. This is an example of pseudoasymmetic cases.

For H^2X^2, a $\mathbf{C}_{2v}$-molecule and a $\mathbf{C}_2'$-molecule can exist so that they are characterized, respectively, by an orbit of $\mathbf{C}_{2v}$-assemblies and an orbit of $\mathbf{C}_2'$-assemblies in assembled mandalas. Hence, the two-membered orbit of $\mathbf{C}_{2v}$-assemblies in an assembled mandala is characterized by an FPV = (2, 2, 0, 2, 0, 2, 0, 0) which corresponds to the LCR $\mathbf{D}_{2d}(/\mathbf{C}_{2v})$. The four-membered orbit of $\mathbf{C}_2'$-assemblies, which is governed by the LCR $\mathbf{D}_{2d}(/\mathbf{C}_2')$, is characterized by an FPV = (4, 0, 2, 0, 0, 0, 0, 0) for another assembled mandala. It follows that the case of H^2X^2 is characterized by the summed FPV = (6, 2, 2, 2, 0, 2, 0, 0). The summed FPV gives the coefficients for the terms $6\text{H}^2\text{X}^2$ for $\mathbf{D}_{2d}$, $2\text{H}^2\text{X}^2$ for $\mathbf{C}_2$, etc.

Next, we consider the case of H^2p^2 ($\text{H}^2\overline{\text{p}}^2$), which generates a di-p-substituted allene derivative of $\mathbf{C}_2'$-symmetry (**102**), as shown in figure 23. The symmetry operations of $\mathbf{D}_{2d}$ transform the reference transformula **102** (f_1) into the transformulas (**102**–**109**, i.e., f_1–f_8) to give a reduced mandala (figure 23). The

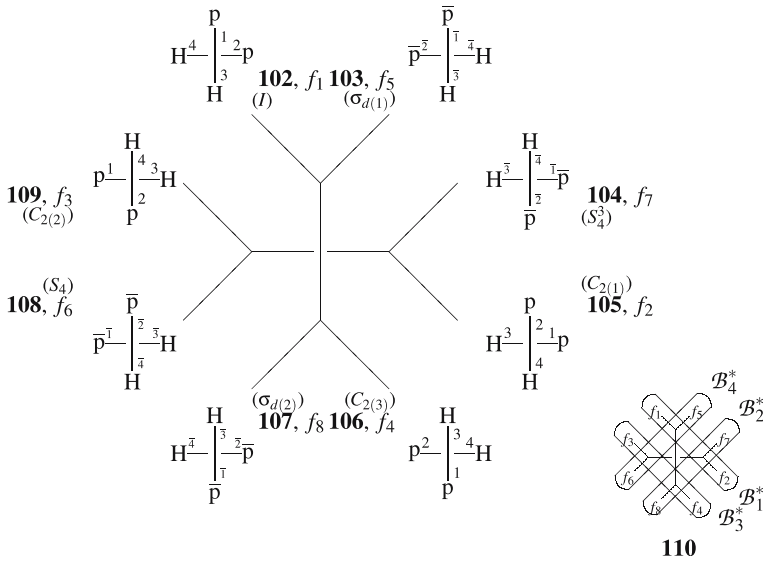

Figure 23. Reduced mandala with $\mathbf{C}'_2$-transformulas derived from an allene skeleton, the vertices of which construct an orbit governed by the subduction of the RCR $(\mathbf{C}_s\backslash)\mathbf{D}_{2d} \downarrow \mathbf{C}'_2 = 2(\mathbf{C}_1\backslash)\mathbf{C}'_2)$. The $\mathbf{C}'_2$-transformulas are assembled into four assemblies (**102/105**, **106/109**, **103/108**, and **104/107**), which construct a four-membered orbit governed by the LCR $\mathbf{D}_{2d}(/\mathbf{C}'_2)$. The orbit (representing a di-X-allene molecule) is characterized by marks (4, 0, 2, 0, 0, 0, 0, 0).

mandala is assembled to give four assemblies, $\mathcal{B}_1^* = \{f_1, f_2\}$ (**102/105**), $\mathcal{B}_4^* = \{f_5, f_6\}$ (**103/108**), $\mathcal{B}_3^* = \{f_4, f_3\}$ (**106/109**), and $\mathcal{B}_2^* = \{f_8, f_7\}$ (**104/107**), each of which represents a $\mathbf{C}'_2$-molecule permuted under $\mathbf{D}_{2d}$.

The resulting set of the four assemblies, i.e., $\mathcal{B}^* = \{\mathcal{B}_1^*, \mathcal{B}_4^*, \mathcal{B}_3^*, \mathcal{B}_2^*\}$, is an orbit governed by the LCR $\mathbf{D}_{2d}(/\mathbf{C}'_2)$ as shown in **110**. The four-membered $\mathbf{D}_{2d}(/\mathbf{C}'_2)$-orbit ($\mathcal{B}^*$) is fixed by the restriction into each subgroup of $\mathbf{D}_{2d}$ to give an FPV = (4, 0, 2, 0, 0, 0, 0, 0). Because the term H^2p^2 (for $\mathcal{B}_1^*$ and $\mathcal{B}_3^*$) is transformed into $H^2\overline{p}^2$ (for $\mathcal{B}_2^*$ and $\mathcal{B}_4^*$) by improper rotations, each fixed point (in an abstract meaning) should be counted by using the term $(1/2)(H^2p^2 + H^2\overline{p}^2)$ as a unit. Hence, the FPV is represented by the terms $(4/2)(H^2p^2 + H^2\overline{p}^2)$ for $\mathbf{D}_{2d}$, $(2/2)(H^2p^2 + H^2\overline{p}^2)$ for $\mathbf{C}'_2$, etc.

There exists another di-p-substituted allene derivative (**111**) with H^2p^2 ($H^2\overline{p}^2$), which belongs to $\mathbf{C}_2$-symmetry, as shown in figure 24. Thus, the symmetry operations of $\mathbf{D}_{2d}$ transform **111** (f_1) into the transformulas (**111–118**, i.e., f_1–f_8) to produce the corresponding reduced mandala with assemblage (figure 24).

The resulting set of the four assemblies, i.e., $\mathcal{C}_1^* = \{f_1, f_4\}$ (**111/115**), $\mathcal{C}_2^* = \{f_5, f_8\}$ (**112/116**), $\mathcal{C}_3^* = \{f_7, f_6\}$ (**113/117**), and $\mathcal{C}_4^* = \{f_2, f_3\}$ (**114/118**), is an orbit governed by the LCR $\mathbf{D}_{2d}(/\mathbf{C}_2)$. The four-membered $\mathbf{D}_{2d}(/\mathbf{C}_2)$-orbit, i.e., $\mathcal{C}^* = \{\mathcal{C}_1^*, \mathcal{C}_2^*, \mathcal{C}_3^*, \mathcal{C}_4^*\}$, in the simplified reduced mandala (**119**) is fixed by the

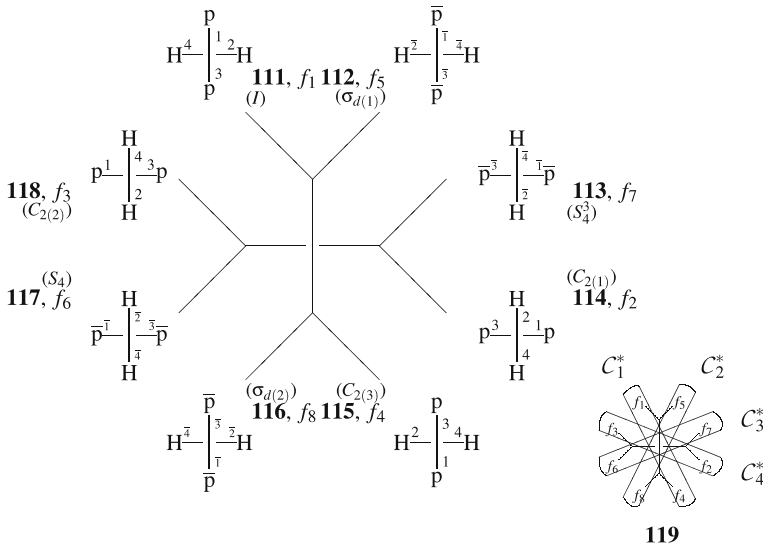

Figure 24. Reduced mandala with $\mathbf{C}_2$-transformulas derived from an allene skeleton, the vertices of which construct an orbit governed by the subduction of the RCR $(\mathbf{C}_s\backslash)\mathbf{D}_{2d} \downarrow \mathbf{C}_2 = 2(\mathbf{C}_1\backslash)\mathbf{C}_2$. The $\mathbf{C}_2$-transformulas are assembled into four assemblies (**111/115**, **112/116**, **113/117**, and **114/118**), which construct a four-membered orbit governed by the LCR $\mathbf{D}_{2d}(/\mathbf{C}_2)$. The orbit (representing a di-p-allene molecule) is characterized by marks (4, 4, 0, 0, 0, 0, 0, 0).

restriction into each subgroup of $\mathbf{D}_{2d}$ to give an FPV = (4, 4, 0, 0, 0, 0, 0, 0). Because the term H^2p^2 (for $\mathcal{C}_1^*$ and $\mathcal{C}_4^*$) is transformed into $H^2\overline{p}^2$ (for $\mathcal{C}_2^*$ and $\mathcal{C}_3^*$) by improper rotations, each fixed point (in an abstract meaning) should be counted by using the term $(1/2)(H^2p^2 + H^2\overline{p}^2)$ as a unit. Hence, The FPV is represented by the terms $(4/2)(H^2p^2 + H^2\overline{p}^2)$ for $\mathbf{D}_{2d}$, $(4/2)(H^2p^2 + H^2\overline{p}^2)$ for $\mathbf{C}_2$, etc.

In stereoisomer enumeration, the two cases of H^2p^2 ($H^2\overline{p}^2$) shown in figures 23 and 24 appear at the same time so as to give a summed FPV = (8, 4, 2, 0, 0, 0, 0, 0). Hence The summed FPV is represented by the terms $(8/2)(H^2p^2 + H^2\overline{p}^2)$ for $\mathbf{D}_{2d}$, $(4/2)(H^2p^2 + H^2\overline{p}^2)$ for $\mathbf{C}_2$, $(2/2)(H^2p^2 + H^2\overline{p}^2)$ for $\mathbf{C}_2'$, etc.

The above-described procedure for evaluating summed FPVs can easily be extended into general cases, in which a given skeleton of **G**-symmetry contains one or more orbits $\mathcal{O}^{(\alpha)}$ of substitution positions. The orbit $\mathcal{O}^{(\alpha)}$ accommodates achiral ligands selected from the following set:

$$\mathbf{X}^{(\alpha)} = \{X_1, X_2, \ldots, X_x\} \tag{81}$$

as well as chiral ligands selected from the following set:

$$\mathbf{p}^{(\alpha)} = \{p_1, p_2, \ldots, p_p; \quad \overline{p}_1, \overline{p}_2, \ldots, \overline{p}_p\}, \tag{82}$$

where p_i and $\overline{\mathrm{p}}_i$ represent a pair of enantiomers ($i = 1, 2, \ldots, p$). Note that, although each ligand should be specified by the index α, its specification is omitted for the sake of simplicity. When the orbit $\mathcal{O}^{(\alpha)}$ accommodates θ_1 of $\mathrm{X}_1, \ldots, \theta_x$ of X_x; θ'_1 of $\mathrm{p}_1, \ldots, \theta'_p$ of p_p; and θ''_1 of $\overline{\mathrm{p}}_1, \ldots, \theta''_p$ of $\overline{\mathrm{p}}_p$, the corresponding weight (molecular formula) is represented by the following equation:

$$W_\theta^{(\alpha)} = \mathrm{X}_1^{\theta_1} \ldots \mathrm{X}_x^{\theta_x} \mathrm{p}_1^{\theta'_1} \ldots \mathrm{p}_p^{\theta'_p} \overline{\mathrm{p}}_1^{\theta''_1} \ldots \overline{\mathrm{p}}_p^{\theta''_p}, \tag{83}$$

where the powers satisfies the following partition:

$$[\theta]^{(\alpha)}: \quad (\theta_1 + \cdots + \theta_x) + (\theta'_1 + \cdots + \theta'_p) + (\theta''_1 + \cdots + \theta''_p) = |\mathcal{O}^{(\alpha)}|. \tag{84}$$

Because the sets represented by equations (81) and (82) may be different according to the index α for $\mathcal{O}^{(\alpha)}$, the weight (equation (83)) and the partition (equation (84)) depend on the index α. As result, the total weight is represented as follows:

$$W_\theta = \prod_\alpha W_\theta^{(\alpha)}. \tag{85}$$

Strictly speaking, equation (85) should be modified to treat chiral molecules as well as achiral ones. Thus, the total weight is represented as follows:

$$W_\theta = \frac{1}{2}\left(\prod_\alpha W_\theta^{(\alpha)} + \prod_\alpha \overline{W}_\theta^{(\alpha)} \right), \tag{86}$$

where we place

$$\overline{W}_\theta^{(\alpha)} = \mathrm{X}_1^{\theta_1} \ldots \mathrm{X}_x^{\theta_x} \mathrm{p}_1^{\theta''_1} \ldots \mathrm{p}_p^{\theta''_p} \overline{\mathrm{p}}_1^{\theta'_1} \ldots \overline{\mathrm{p}}_p^{\theta'_p}. \tag{87}$$

Obviously, if we place $\theta'_i = \theta''_i$ ($i = 1, 2, \ldots, p$), we obtain $W_\theta^{(\alpha)} = \overline{W}_\theta^{(\alpha)}$ so as to give equation (85).

Suppose that the **G**-symmetry of the skeleton is characterized by the following SSG:

$$\mathrm{SSG}_{\mathbf{G}} = \{\mathbf{G}_1 (= \mathbf{C}_1), \mathbf{G}_2, \ldots, \mathbf{G}_i, \ldots, \mathbf{G}_s (= \mathbf{G})\}, \tag{88}$$

where we place $|\mathbf{G}_1| \leqslant |\mathbf{G}_2| \leqslant \cdots \leqslant |\mathbf{G}_i| \leqslant \cdots \leqslant |\mathbf{G}_s|$ and the corresponding mark table is represented as follows:

$$M_{\mathbf{G}} = (m_{ij}) = \begin{pmatrix} m_{11} & \cdots & m_{1j} & \cdots & m_{1s} \\ \vdots & & \vdots & & \vdots \\ m_{i1} & \cdots & m_{ij} & \cdots & m_{is} \\ \vdots & & \vdots & & \vdots \\ m_{s1} & \cdots & m_{sj} & \cdots & m_{ss} \end{pmatrix}. \tag{89}$$

Mark table ($M_{\mathbf{G}}$)

Let the symbol $B_{\theta i}$ represent the number of $\mathbf{G}_i$-molecules with the weight W_θ. Because each of the $\mathbf{G}_i$-molecules is characterized by the FPV = $(m_{i1}, \ldots, m_{ij}, \ldots, m_{is})$, the corresponding summed FPV = $(\rho_{\theta 1}, \ldots, \rho_{\theta j}, \ldots, \rho_{\theta s})$ is represented as follows:

$$(\rho_{\theta 1}, \ldots, \rho_{\theta j}, \ldots, \rho_{\theta s}) = \left(\sum_i B_{\theta i} m_{i1}, \ldots, \sum_i B_{\theta i} m_{ij}, \ldots, \sum_i B_{\theta i} m_{is} \right), \quad (90)$$

where $\mathbf{G}_i$ runs over the SSG (equation (88)) for a fixed W_θ. When the $[\theta]$ runs over the partition shown in equation (84), we obtain the following matrix representation:

$$\begin{pmatrix} \rho_{11} & \cdots & \rho_{1j} & \cdots & \rho_{1s} \\ \rho_{21} & \cdots & \rho_{2j} & \cdots & \rho_{2s} \\ \vdots & & \vdots & & \vdots \\ \rho_{\theta 1} & \cdots & \rho_{\theta j} & \cdots & \rho_{\theta s} \\ \vdots & & \vdots & & \vdots \\ \rho_{|\theta|1} & \cdots & \rho_{|\theta|j} & \cdots & \rho_{|\theta|s} \end{pmatrix} = \begin{pmatrix} B_{11} & \cdots & B_{1i} & \cdots & B_{1s} \\ B_{21} & \cdots & B_{2i} & \cdots & B_{2s} \\ \vdots & & \vdots & & \vdots \\ B_{\theta 1} & \cdots & B_{\theta i} & \cdots & B_{\theta s} \\ \vdots & & \vdots & & \vdots \\ B_{|\theta|1} & \cdots & B_{|\theta|i} & \cdots & B_{|\theta|s} \end{pmatrix} \begin{pmatrix} m_{11} & \cdots & m_{1j} & \cdots & m_{1s} \\ \vdots & & \vdots & & \vdots \\ m_{i1} & \cdots & m_{ij} & \cdots & m_{is} \\ \vdots & & \vdots & & \vdots \\ m_{s1} & \cdots & m_{sj} & \cdots & m_{ss} \end{pmatrix}, \quad (91)$$

FPM ICM Mark table ($M_{\mathbf{G}}$)

where the first matrix is called *a* FPM and the second is called *an isomer-counting matrix* (ICM).

Because the mark table has its inverse, we place $M_{\mathbf{G}}^{-1} = (\overline{m}_{ij})$. Thereby, equation (91) is converted into the following equation:

$$\begin{pmatrix} B_{11} & \cdots & B_{1i} & \cdots & B_{1s} \\ B_{21} & \cdots & B_{2i} & \cdots & B_{2s} \\ \vdots & & \vdots & & \vdots \\ B_{\theta 1} & \cdots & B_{\theta i} & \cdots & B_{\theta s} \\ \vdots & & \vdots & & \vdots \\ B_{|\theta|1} & \cdots & B_{|\theta|i} & \cdots & B_{|\theta|s} \end{pmatrix} = \begin{pmatrix} \rho_{11} & \cdots & \rho_{1j} & \cdots & \rho_{1s} \\ \rho_{21} & \cdots & \rho_{2j} & \cdots & \rho_{2s} \\ \vdots & & \vdots & & \vdots \\ \rho_{\theta 1} & \cdots & \rho_{\theta j} & \cdots & \rho_{\theta s} \\ \vdots & & \vdots & & \vdots \\ \rho_{|\theta|1} & \cdots & \rho_{|\theta|j} & \cdots & \rho_{|\theta|s} \end{pmatrix} \begin{pmatrix} \overline{m}_{11} & \cdots & \overline{m}_{i1} & \cdots & \overline{m}_{s1} \\ \vdots & & \vdots & & \vdots \\ \overline{m}_{1j} & \cdots & \overline{m}_{ij} & \cdots & \overline{m}_{sj} \\ \vdots & & \vdots & & \vdots \\ \overline{m}_{1s} & \cdots & \overline{m}_{is} & \cdots & \overline{m}_{ss} \end{pmatrix}. \quad (92)$$

ICM FPM Inverse mark table ($M_{\mathbf{G}}^{-1}$)

This equation means that, if we evaluate each element $\rho_{\theta j}$ of the FPM, we are able to calculate the number $B_{\theta i}$ of the ICM. For this purpose, we shall adopt the column view of the FPM, as discussed in the next section, where we take account of the column vector $(\rho_{1j}, \rho_{2j}, \ldots, \rho_{|\theta|j})^T$ for the jth column of the FPV.

5.2. Column view for evaluating fixed-point vectors

For the column view of the FPM appearing in equation (92), we should remember that the jth column $(\rho_{1j}, \rho_{2j}, \ldots, \rho_{|\theta|j})^T$ is concerned with the subduction into the subgroup $\mathbf{G}_j$. It is convenient that the jth column is evaluated in the form of a generating function represented by $\sum_{\theta} \rho_{\theta j} W_\theta$ as shown in the following example.

Example 23. According to theorem 7, one reduced mandala with $\mathbf{C}_s$-assemblage (**83**) corresponds to one $\mathbf{C}_s$-molecule. The $\mathbf{C}_s$-assemblage results in the subduction of the $(\mathbf{C}_s\backslash)\mathbf{D}_{2d}$-orbit, which is represented by $(\mathbf{C}_s\backslash)\mathbf{D}_{2d} \downarrow \mathbf{C}_s = 2(\mathbf{C}_s\backslash)\mathbf{C}_s + (\mathbf{C}_1\backslash)\mathbf{C}_s$. The corresponding USCI-CF $(a_1^2 c_2)$ controls the substitution mode of atoms and/or (pro)ligands according to its sphericity indices (i.e., the chirality fittingness of the orbit at issue).

Let us consider H, X, p, and $\overline{\text{p}}$ as substituents. Then, a H^3X-molecule belongs to $\mathbf{C}_s$-symmetry, as found in figure 21, where two of the one-membered homospheric orbit characterized by the sphericity index a_1 accommodate H and X distinctly, while the two-membered enantiospheric orbit characterized by c_2 accommodates a set of two hydrogens. This substitution process is shown in the top scheme of figure 25, where two transformulas (**84** and **88**) ascribed to the same $\mathbf{C}_s$-molecule are generated. Note that the subduction into $\mathbf{C}_s$ corresponds to the $\mathbf{C}_s$-assemblage selecting two intermediate transformulas, i.e., **75** (f_1) and **79** (f_4), where the substitution obeys a function, $f(1) = \text{X}, f(2) = f(3) = f(4) = \text{H}$. This means that the corresponding mark is equal to 2, which is expressed by the term $2H^3X$.

On the other hand, the substitution due to a function f, i.e., $f(1) = X, f(2) = \text{p}, f(3) = \overline{\text{p}}$, and $f(4) = \text{H}$ (cf. figure 22), generates two transformulas (**93** and **97**), which are ascribed to another $\mathbf{C}_s$-molecule having a molecular formula $HXp\overline{p}$ (the middle scheme of figure 25). The two of the one-membered homospheric orbits characterized by the sphericity index a_1 accommodate H and X distinctly, whereas the two-membered enantiospheric orbit characterized by c_2 accommodates a pair of p and $\overline{\text{p}}$. This means that the corresponding mark is equal to 2, which is expressed by the term $2HXp\overline{p}$. Another $\mathbf{C}_s$-molecule with the molecular formula $HXp\overline{p}$ can be generated by a function, $f(1) = \text{X}, f(2) = \overline{\text{p}}, f(3) = \text{p}$, and $f(4) = \text{H}$. The resulting two transformulas (**120** and **121**) shown as the bottom scheme of figure 25) indicates that the corresponding mark is equal to 2, which is expressed by the term $2HXp\overline{p}$. The middle scheme and the bottom one show pseudoasymmetry, which is expressed by the summed term $4HXp\overline{p}$.

The above discussions indicate that the one-membered homospheric orbit permits H and X in agreement with the sphericity index a_1, while the two-membered enantiospheric orbit permits two Hs, two Xs, or a pair of p and $\overline{\text{p}}$ in

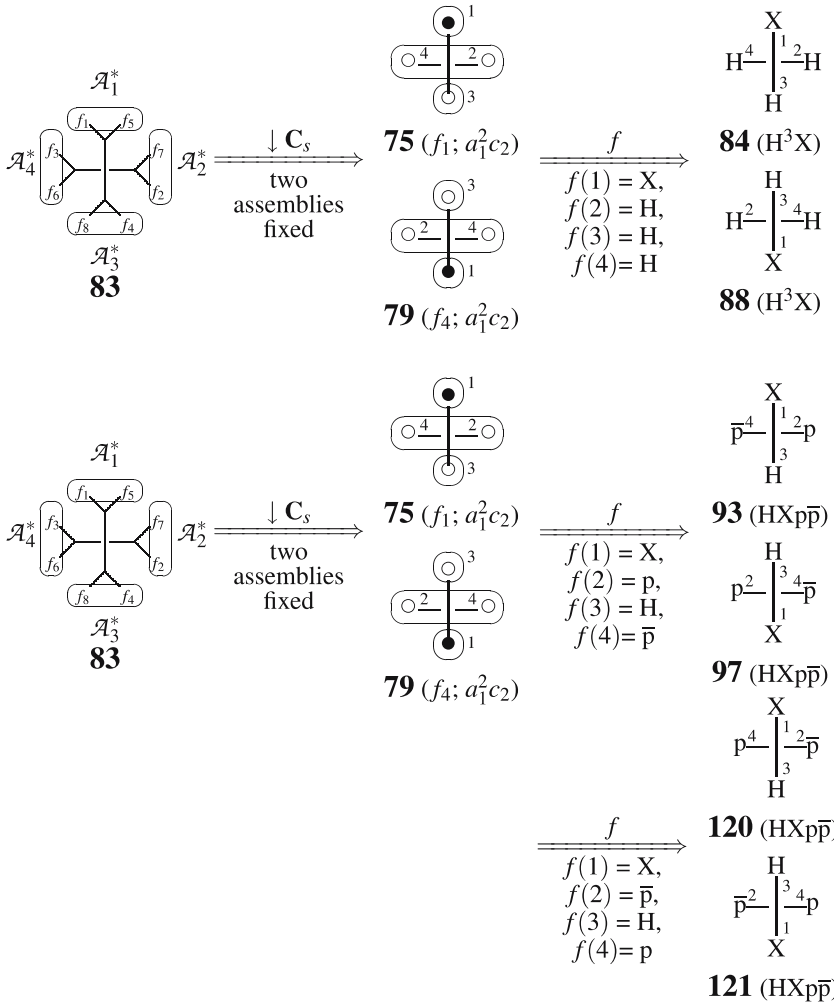

Figure 25. Two transformulas (**84** and **84**) ascribed to a $\mathbf{C}_s$-molecule with the formula H^3X as well as a set of two transformulas (**93** and **97**) and another set of two transformulas (**120** and **121**), both ascribed to $\mathbf{C}_s$-molecules with the formula $HXp\overline{p}$.

agreement with the sphericity index c_2. The modes of permission are represented by the following ligand inventories:

$$a_1 = \mathrm{H} + \mathrm{X}, \tag{93}$$

$$c_2 = \mathrm{H}^2 + \mathrm{X}^2 + 2\mathrm{p}\overline{\mathrm{p}}. \tag{94}$$

These are introduced into the USCI-CF to give the following generating function:

$$a_1^2 c_2 = (\mathrm{H} + \mathrm{X})^2(\mathrm{H}^2 + \mathrm{X}^2 + 2\mathrm{p}\overline{\mathrm{p}}) \\ = (\mathrm{H}^4 + \mathrm{X}^4) + (2\mathrm{H}^3\mathrm{X} + 2\mathrm{H}\mathrm{X}^3) + 2\mathrm{H}^2\mathrm{X}^2 + 2\mathrm{H}^2\mathrm{p}\overline{\mathrm{p}} + 2\mathrm{X}^2\mathrm{p}\overline{\mathrm{p}} + 4\mathrm{H}\mathrm{X}\mathrm{p}\overline{\mathrm{p}}. \tag{95}$$

The coefficient 2 of the term $\mathrm{H}^3\mathrm{X}$ and the coefficient 4 of the term $\mathrm{HXp}\overline{\mathrm{p}}$ are identical with the values evaluated above in detail. The generation function shown by 95 exemplifies a mode of column view, which corresponds to the general equation $\sum_{\theta} \rho_{\theta j} W_{\theta}$.

It should be noted that equation (95) contains the terms H^4 and X^4, which are ascribed to $\mathbf{C}_{2v}$-molecules. Because the $\mathbf{C}_{2v}$ is a supergroup of $\mathbf{C}_s$, the $\mathbf{C}_{2v}$-molecules are also fixed under the subduction into $\mathbf{C}_s$ so as to give the mark 1 as the coefficients of the terms H^4 and X^4. □

The column view described in example 23 can be extended into general cases in which one or more orbits of substitution positions participate in stereoisomer enumeration. Suppose that the orbit $\mathcal{O}^{(\alpha)}$ governed by the RCR $(\mathbf{G}_{\ell}\backslash)\mathbf{G}$ is restricted into its subgroup $\mathbf{G}_j$, where the restriction is determined by the subduction $(\mathbf{G}_{\ell}\backslash)\mathbf{G} \downarrow \mathbf{G}_j$. The subduction $(\mathbf{G}_{\ell}\backslash)\mathbf{G} \downarrow \mathbf{G}_j$ is calculated according to equation (57) so as to be characterized by the corresponding USCI-CF, i.e.,

$$\text{USCI-CF}(\mathbf{G}_j; \$_d)^{(\alpha)}, \tag{96}$$

where the symbol $\$_d$ indicates a_d, b_d, or c_d (cf. example 5). When the orbit $\mathcal{O}^{(\alpha)}$ runs to cover all of the substitution positions of the skeleton (i.e., $\mathcal{O} = \bigcup_{\alpha} \mathcal{O}^{(\alpha)}$), the multiplication of the USCI-CFs (equation (96)) gives the following product:

$$\text{SCI-CF}(\mathbf{G}_j; \$_d) = \prod_{\alpha} \text{USCI-CF}(\mathbf{G}_j; \$_d)^{(\alpha)}, \tag{97}$$

which are called *a subduced cycle index with chirality fittingness* (SCI-CF) according to Chapter 19 of Fujita's book [12]. By using the SCI-CF (equation (97)), the column view for the FPM provides us with the following theorem:

Theorem 8. Substituents are selected from the sets represented by equations (81) and (82). The weight (equation (83)) and the partition (equation (84)) are used to characterize stereoisomers to be enumerated. A generating function for calculating $\rho_{\theta j}$ (equation (91) or equation (92)) is obtained as follows:

$$\sum_{[\theta]} \rho_{\theta j} W_{\theta} = \text{SCI-CF}(\mathbf{G}_j; \$_d), \tag{98}$$

where the sphericity indices ($\$_d = a_d, b_d$, or c_d) in the SCI-CF are substituted by the following ligand inventories:

$$a_d^{(\alpha)} = \mathrm{X}_1^d + \cdots + \mathrm{X}_x^d, \tag{99}$$

$$c_d^{(\alpha)} = \mathrm{X}_1^d + \cdots + \mathrm{X}_x^d + 2(\mathrm{p}_1^{d/2}\overline{\mathrm{p}}_1^{d/2} + \cdots \mathrm{p}_p^{d/2}\overline{\mathrm{p}}_p^{d/2}), \tag{100}$$

$$b_d^{(\alpha)} = (\mathrm{X}_1^d + \cdots + \mathrm{X}_x^d) + (\mathrm{p}_1^d + \cdots + \mathrm{p}_p^d) + (\overline{\mathrm{p}}_1^d + \cdots + \overline{\mathrm{p}}_p^d), \tag{101}$$

where the index α of each inventory corresponds to the USCI-CFs shown on the right-hand side of equation (97).

This theorem is equivalent to lemma 19.2 of Fujita's book [12]. The ligand inventories used in theorem 8 can be varied for every orbits $\mathcal{O}^{(\alpha)}$, as discussed in Chapters 14 and 19 of Fujita's book [12].

Theorem 8 gives the values for the jth column $(\rho_{1j}, \rho_{2j}, \ldots, \rho_{|\theta|j})^T$, which is concerned with the subduction into the subgroup $\mathbf{G}_j$. By moving j from 1 to s, all of the values of $\rho_{\theta j}$ in the FPM (equation (92)) are calculated. Thereby, the ICM is calculated by means of equation (92). The procedure described here is a diagrammatical formulation of *the SCI method*, which has been alternatively disclosed in terms of a more mathematical formulation in Chapter 19 of Fujita's book [12].

6. Reordered multiplication tables

Mandalas of **G**-symmetry can be directly correlated to the multiplication table of the **G**. For this type of correlation, we have to consider reordered multiplication tables. Thereby, the mandalas clarify concurrent behaviors of RCRs and LCRs through such reordered multiplication tables.

Example 24. The reduced mandala (**101**) shown in figure 22, where the reduction is based on the $\mathbf{C}_s$-segmentation and the subduction stems from the $\mathbf{C}_s$-assemblage, is correlated to the reordered multiplication table shown in figure 26. According to the $\mathbf{C}_s$-segmentation, the rows of the multiplication table (figure 2) are segmented in terms of the right coset decomposition shown in equation (20). The resulting right cosets correspond to the (secondary) positions {1–4} (cf. figure 19), which are generated by the reduction of the segments $\mathcal{A}_1, \mathcal{A}_2, \mathcal{A}_3$, and $\mathcal{A}_4$ (cf. figure 17). This correspondence is shown in the left-most part of figure 26.

Then, the columns of the multiplication table (figure 2) are divided (assembled) in terms of the left coset decomposition shown in equation (43). By using the function f (i.e., $f(1) = \mathrm{X}$, $f(2) = \mathrm{p}$, and $f(3) = \mathrm{H}$, $f(4) = \mathrm{p}$) or by placing X on $\mathcal{A}_1$, p on $\mathcal{A}_2$, H on $\mathcal{A}_3$, and p on $\mathcal{A}_4$, the transformulas (**93**–**100**) are generated as shown in figure 22. Each of the transformulas (**93**–**100**) corresponds

second operation			first operation: $I\mathbf{C}_s$		$C_{2(1)}\mathbf{C}_s$		$C_{2(3)}\mathbf{C}_s$		$C_{2(2)}\mathbf{C}_s$	
			1	5	2	7	4	8	3	6
			X		p ($\overline{\mathrm{p}}$)		H		$\overline{\mathrm{p}}$ ($\overline{\overline{\mathrm{p}}}$)	
$\mathbf{C}_sI$	I	1	1	5	2	7	4	8	3	6
$\mathcal{A}_1$	$\sigma_{d(1)}$	5	5	1	6	3	8	4	7	2
			p ($\overline{\mathrm{p}}$)		X		$\overline{\mathrm{p}}$ ($\overline{\overline{\mathrm{p}}}$)		H	
$\mathbf{C}_sC_{2(1)}$	$C_{2(1)}$	2	2	7	1	5	3	6	4	8
$\mathcal{A}_2$	S_4	6	6	3	5	1	7	2	8	4
			H		$\overline{\mathrm{p}}$ ($\overline{\overline{\mathrm{p}}}$)		X		p ($\overline{\mathrm{p}}$)	
$\mathbf{C}_sC_{2(3)}$	$C_{2(3)}$	4	4	8	3	6	1	5	2	7
$\mathcal{A}_3$	$\sigma_{d(2)}$	8	8	4	7	2	5	1	6	3
			$\overline{\mathrm{p}}$ ($\overline{\overline{\mathrm{p}}}$)		H		p ($\overline{\mathrm{p}}$)		X	
$\mathbf{C}_sC_{2(2)}$	$C_{2(2)}$	3	3	6	4	8	2	7	1	5
$\mathcal{A}_4$	S_4^3	7	7	2	8	4	6	3	5	1
Fig. 22			**93**	**94**	**96**	**95**	**97**	**98**	**100**	**99**
			(f_1)	(f_5)	(f_2)	(f_7)	(f_4)	(f_8)	(f_3)	(f_6)
			$\mathcal{A}_1^*$		$\mathcal{A}_2^*$		$\mathcal{A}_3^*$		$\mathcal{A}_4^*$	

Figure 26. Reordered multiplication table of $\mathbf{D}_{2d}$ for showing a reduced mandala with $\mathbf{C}_s$-segmentation and $\mathbf{C}_s$-assemblage (cf. figure 22).

to each column of the reordered multiplication table (figure 26). The division of the columns corresponds to the $\mathbf{C}_s$-assemblage, which generates the assemblies $\mathcal{A}_1^*$, $\mathcal{A}_2^*$, $\mathcal{A}_3^*$, and $\mathcal{A}_4^*$ (cf. **101**), as shown in the bottom part of the reordered multiplication table (figure 26). □

Example 25. Let us next examine the reduced mandala shown in figure 23, where the reduction is based on the $\mathbf{C}_s$-segmentation and the subduction stems from the $\mathbf{C}_2'$-assemblage. The reduced mandala is correlated to the reordered multiplication shown in figure 27.

On the same line as example 24, the rows of the multiplication table (figure 2) are segmented according to the $\mathbf{C}_s$-segmentation, which is based on the right coset decomposition shown in equation (20). The correspondence of the resulting right cosets to the (secondary) positions $\{1, 2, 3, 4\}$ (cf. figure 23) is shown in the left-most part of figure 27. The numbering of the positions is correlated to that of the segments, $\mathcal{A}_1, \mathcal{A}_2, \mathcal{A}_3$, and $\mathcal{A}_4$.

The columns of the multiplication table (figure 2) are divided (assembled) in terms of the left coset decomposition:

$$\mathbf{D}_{2d} = \mathbf{C}_2' + S_4^3\mathbf{C}_2' + C_{2(3)}\mathbf{C}_2' + S_4\mathbf{C}_2' \tag{102}$$

$$= \{1, 2\} + \{7, 8\} + \{4, 3\} + \{6, 5\}, \tag{103}$$

second operation			first operation: $I\mathbf{C}'_2$		$S_4^3\mathbf{C}'_2$		$C_{2(3)}\mathbf{C}'_2$		$S_4\mathbf{C}'_2$	
			1	2	7	8	4	3	6	5
			p ($\overline{\text{p}}$)		H		H		p ($\overline{\text{p}}$)	
$\mathbf{C}_sI$	I	1	1	2	7	8	4	3	6	5
$\mathcal{A}_1$	$\sigma_{d(1)}$	5	5	6	3	4	8	7	2	1
			p ($\overline{\text{p}}$)		p ($\overline{\text{p}}$)		H		H	
$\mathbf{C}_sC_{2(1)}$	$C_{2(1)}$	2	2	1	5	6	3	4	8	7
$\mathcal{A}_2$	S_4	6	6	5	1	2	7	8	4	3
			H		p ($\overline{\text{p}}$)		p ($\overline{\text{p}}$)		H	
$\mathbf{C}_sC_{2(3)}$	$C_{2(3)}$	4	4	3	6	5	1	2	7	8
$\mathcal{A}_3$	$\sigma_{d(2)}$	8	8	7	2	1	5	6	3	4
			H		H		p ($\overline{\text{p}}$)		p ($\overline{\text{p}}$)	
$\mathbf{C}_sC_{2(2)}$	$C_{2(2)}$	3	3	4	8	7	2	1	5	6
$\mathcal{A}_4$	S_4^3	7	7	8	4	3	6	5	1	2
Fig. 23			**102**	**103**	**105**	**104**	**106**	**107**	**109**	**108**
			(f_1)	(f_2)	(f_7)	(f_8)	(f_4)	(f_3)	(f_6)	(f_5)
			$\mathcal{B}_1^*$		$\mathcal{B}_2^*$		$\mathcal{B}_3^*$		$\mathcal{B}_4^*$	

Figure 27. Reordered multiplication table of $\mathbf{D}_{2d}$ for showing a reduced mandala with $\mathbf{C}_s$-segmentation and $\mathbf{C}'_2$-assemblage (cf. figure 23).

which is shown at the top part of figure 27. By using the function f (i.e., $f(1) =$ p, $f(2) =$ p, and $f(3) =$ H, $f(4) =$ H) or by placing p on $\mathcal{A}_1$, p on $\mathcal{A}_2$, H on $\mathcal{A}_3$, and H on $\mathcal{A}_4$, the transformulas (**102**–**109**) are generated as shown in figure 23. The transformulas (**102**–**109**), respectively, correspond to the columns of the reordered multiplication table (figure 27). The division of the columns corresponds to the $\mathbf{C}'_2$-assemblage, which generates the assemblies $\mathcal{B}_1^*$, $\mathcal{B}_2^*$, $\mathcal{B}_3^*$, and $\mathcal{B}_4^*$ (cf. **110**). These results are shown in the bottom part of the reordered multiplication table (figure 27). □

The results described in examples 24 and 25 can be easily extended into general cases, as summarized in a theorem:

Theorem 9. A mandala of **G**-symmetry with an **H**-segmentation and an **K**-assemblage is correlated to the reordered multiplication of **G** in which the rows (second operations) are divided (segmented) on the basis of the right coset decomposition of **G** by **H** and the columns (first operations) are divided (assembled) on the basis of the left coset decomposition of **G** by **K**. The mandala of **G**-symmetry with an **H**-segmentation and a **K**-assemblage represents one molecule of the **K**-symmetry which is derived from a **G**-skeleton with a (**H**\)**G**-orbit of substitution positions.

Theorem 9 holds true for cases in which the **G**-skeleton has one or more orbits represented by $\sum_{\mathrm{H}} \alpha_{\mathrm{H}}(\mathbf{H}\backslash)\mathbf{G}$, where the symbol α_{H} represents the multiplicity of the $(\mathbf{H}\backslash)\mathbf{G}$-orbits.

7. Conclusions

Right coset representations $(\mathbf{H}\backslash)\mathbf{G}$ and LCR $\mathbf{G}(/\mathbf{H})$ are introduced by starting from the right and left coset decompositions of the group **G** by its subgroup **H**. The sphericity of the RCR (or the LCR) is defined as being homospheric for an achiral group **G** and an achiral group **H**, being enantiospheric for an achiral group **G** and a chiral group **H**, and being hemispheric for a chiral group **G** and a chiral group **H**. After defining the mark of each RCR or LCR during the restriction into a subgroup **K** of **G**, the **K** is moved to cover **G** up to conjugate subgroups so as to give a FPV for the RCR (or the LCR).

A regular body of **G**-symmetry is defined as a diagrammatical expression for a RRR $(\mathbf{C}_1\backslash)\mathbf{G}$, which is an extreme case of RCRs. The **H**-segmentation of the regular body as a reference is defined to specify the RCR $(\mathbf{H}\backslash)\mathbf{G}$, which controls $|\mathbf{G}|/|\mathbf{H}|$ of the resulting **H**-segments. A mandala is defined as a nested regular body of **G**-symmetry, in which regular bodies generated by every symmetry operations of **G** on the reference regular body are placed on the vertices of a hypothetical regular body of **G**-symmetry. By regarding each **H**-segment as a substitution position, the **H**-segmented regular body is reduced into a reduced regular body, which generates a reduced mandala as a diagrammatical expression of a molecule.

The effect of a **K**-subduction on regular bodies of a mandala (or a reduced mandala) results in the **K**-assemblage of the mandala (or the reduced mandala), where $|\mathbf{G}|/|\mathbf{K}|$ of the resulting **K**-assemblies are governed by the LCR $\mathbf{G}(/\mathbf{K})$. The FPV for each mandala (or reduced mandala) in row view and the number of fixed points of **K**-assembled mandalas (or **K**-assembled reduced mandalas) in column view are compared to accomplish combinatorial enumeration of stereoisomers. The relationship between a mandala and a reordered multiplication table is discussed.

It is to be emphasized that regular bodies and their segmentation are diagrammatical tools for discussing intramolecular stereochemistry, while mandalas and their assemblage are diagrammatical tools for discussing intermolecular stereochemistry (stereoisomerism). The subduction of coset representations is concluded to bridge between the regular bodies and the mandalas. Thus, the concept of mandala reinforces the versatility of Fujita's USCI (unit-subduced-cycle-index) approach [12].

References

[1] K. Mislow and M. Raban, Top. Stereochem. 1 (1967) 1–38.
[2] E.L. Eliel, J. Chem. Educ. 57 (1980) 52–55.
[3] K. Mislow and J. Siegel, J. Am. Chem. Soc. 106 (1984) 3319–3328.
[4] E. Eliel and S. H. Wilen, *Stereochemistry of Organic Compounds* (Wiley, New York, 1994).
[5] N. North, *Principles and Applications of Stereochemistry* (Stanley Thornes, Cheltenham, 1998).
[6] D.G. Morris, *Stereochemistry* (Royal Society of Chemistry, Cambridge, 2001).
[7] J. Eames and J. M. Peach, *Stereochemistry at a Glance* (Blackwell, Oxford, 2003).
[8] J. Sheehan, Can. J. Math. 20 (1968) 1068–1076.
[9] J. Brocas, J. Am. Chem. Soc. 108 (1986) 1135–1145.
[10] W. Hässelbarth, Theor. Chim. Acta 67 (1985) 339–367.
[11] C.A. Mead, J. Am. Chem. Soc. 109 (1987) 2130–2137.
[12] S. Fujita, *Symmetry and Combinatorial Enumeration in Chemistry* (Springer-Verlag, Berlin-Heidelberg, 1991).
[13] S. Fujita, Bull. Chem. Soc. Jpn. 63 (1990) 315–327.
[14] S. Fujita, J. Am. Chem. Soc. 112 (1990) 3390–3397.
[15] S. Fujita, Theor. Chim. Acta 76 (1989) 247–268.
[16] S. Fujita, J. Math. Chem. 5 (1990) 121–156.
[17] S. Fujita, Bull. Chem. Soc. Jpn. 63 (1990) 203–215.
[18] S. Fujita, Bull. Chem. Soc. Jpn. 74 (2001) 1585–1603.
[19] S. Fujita, Chem. Rec. 2 (2002) 164–176.
[20] S. Fujita, Bull. Chem. Soc. Jpn. 75 (2002) 1863–1883.
[21] C. A. Mead, J. Am. Chem. Soc. 114 (1992) 4018–4019.
[22] S. El-Basil, *Combinatorial Organic Chemistry, An Educational Approach* (Nova Scientific, New York, 1999).
[23] S. El-Basil, MATCH Commun. Math. Comput. Chem. 46 (2002) 7–23.
[24] S. Fujita, J. Org. Chem. 67 (2002) 6055–6063.
[25] S. Fujita, J. Comput. Chem. Jpn. 3 (2004) 113–120.
[26] S. Fujita, Chem. Educ. J. 8 (2005) Registration No. 8–8.
[27] S. Fujita, Chem. Educ. J. 8 (2005) Registration No. 8–9.
[28] S. Fujita and S. El-Basil, MATCH Commun. Math. Comput. Chem. 46 (2002) 121–135.
[29] S. Fujita and S. El-Basil, J. Math. Chem. 33 (2003) 255–277.
[30] S. Fujita and S. El-Basil, J. Math. Chem. 36 (2004) 211–229.
[31] S. Fujita, MATCH Commun. Math. Comput. Chem. 54 (2005) 251–300.
[32] S. Fujita, MATCH Commun. Math. Comput. Chem. 55 (2006) 5–38.
[33] S. Fujita, MATCH Commun. Math. Comput. Chem. 55 (2006) 237–270.
[34] W. Burnside, *Theory of Groups of Finite Order*, 2nd ed. (Cambridge University Press, Cambridge, 1911).
[35] S. Fujita, Theor. Chem. Acc. 113 (2005) 73–79.
[36] S. Fujita, Theor. Chem. Acc. 113 (2005) 80–86.
[37] S. Fujita, Theor. Chem. Acc. 115 (2006) 37–53.